CR-159499
R80AEG313

National Aeronautics and
Space Administration

CORE COMPRESSOR EXIT STAGE STUDY

Volume III - Data and Performance Report for Screening Test Configurations

by

D.C. Wisler

GENERAL ELECTRIC COMPANY

NOVEMBER 1980

Prepared For

National Aeronautics and Space Administration

Contract No. NAS3-20070
NASA-Lewis Research Center

1. Report No.	2. Government Accession No.	3. Recipient's Catalog No.
NASA CR-159499		

4. Title and Subtitle	5. Report Date
Core Compressor Exit Stage Study Volume III - Data and Performance Report for Screening Test Configurations	November, 1980
	6. Performing Organization Code
7. Author(s)	8. Performing Organization Report No.
D.C. Wisler	R80AEG313
	10. Work Unit No.
9. Performing Organization Name and Address	
General Electric Company Aircraft Engine Group Cincinnati, Ohio 45215	11. Contract or Grant No. NAS3-20070
	13. Type of Report and Period Covered
12. Sponsoring Agency Name and Address	Data Report
NASA-Lewis Research Center 21000 Brookpark Road Cleveland, Ohio 44135	14. Sponsoring Agency Code

15. Supplementary Notes

Project Manager, Dr. Wojiech Rostafinski, Fluid Mechanics and Acoustics Division, NASA-Lewis Research Center, Cleveland, Ohio 44135

16. Abstract

The objective of the Core Compressor Exit Stage Study Program is to develop rear stage blading designs that have lower losses in their endwall boundary layer regions. This report describes the test data and performance results for Rotor B, Stator B, and Stator C - blading designs that offer promise of reducing endwall losses relative to the baseline Stage A. The overall technical approach in this efficiency improvement program utilizes the General Electric Low Speed Research Compressor as the principal investigative tool. All of the tests were conducted using four identical stages of blading so that the test data would be obtained in a true multistage environment.

17. Key Words (Suggested by Author(s))	18. Distribution Statement
Compressor Endwall Secondary Flow	Unclassified - Unlimited

19. Security Classif. (of this report)	20. Security Classif. (of this page)	21. No. of Pages	22. Price*
Unclassified	Unclassified		

* For sale by the National Technical Information Service, Springfield, Virginia 22161

TABLE OF CONTENTS

LIST OF ILLUSTRATIONS

LIST OF ILLUSTRATIONS (Concluded)

LIST OF TABLES

1.0 SUMMARY

The Core Compressor Exit Stage Study Program has the primary objective of developing rear stage blade designs that have improved efficiency by virtue of having lower losses in their endwall boundary layer regions. Blading concepts that offer promise of reducing endwall losses have been evaluated in a multistage environment. This report describes the test data and the performance results obtained from the Screening Tests of Rotor B, Stator B and Stator C - the three rear stage blading designs developed to have improved efficiency. Rotor B uses a meanline in the tip region that unloads the leading edge and loads the trailing edge relative to the baseline Rotor A. Stator B embodies twist gradients in the endwall regions relative to the baseline Stator A. Stator C uses airfoil sections that have reduced trailing edge loading near the endwalls relative to Stator A. The details of these designs are presented in Volume I of this report (Reference I). All testing was conducted in the General Electric Low Speed Research Compressor. The test results for the baseline blading are described in Volume II (Reference 2). The Screening Test results are summarized below.

- Rotor B tested with Stator A showed a 0.3 point improvement in efficiency at the design point relative to the baseline.

- Stator B tested with Rotor A showed a 0.4 to 0.5 point improvement in efficiency at the design point and a significant improvement in the pressure-flow characteristic near stall relative to the baseline.

- Stator C tested with Rotor A showed a slight loss in efficiency at the design point relative to the baseline.

- Rotor B tested with Stator B showed a 0.3 to 0.4 point improvement in efficiency at the design point and a significant improvement in the pressure-flow characteristic near stall relative to the baseline.

2.0 INTRODUCTION

Recent preliminary design studies of advanced turbofan core compressors (Reference 3) have indicated that such compressors must have very high efficiencies, as well as the advantages of compactness, light weight and low cost, in order for advanced overall engine/aircraft systems to have an improved economic payoff. Loss mechanism assessments, such as that of Reference 4, suggest that approximately half of the total loss in a multistage compressor rear stage is associated with the endwall boundary layers. Since only a relatively small amount of past research has been dedicated to the problem of finding improved airfoil shapes for operation in multistage compressor endwall boundary layers, it is believed that substantial improvements in that area are likely. Accordingly, a goal of a 15 percent reduction in rear stage endwall boundary layer losses, compared to current technology levels, has been set. The Core Compressor Exit Stage Study Program is directed at achieving this goal. Blading concepts that offer promise of reducing endwall losses have been evaluated in a multistage environment. The Screening Test data and performance results for this blading are presented in this report.

3.0 TEST APPARATUS AND PROCEDURE

3.1 LOW SPEED RESEARCH COMPRESSOR TEST FACILITY

The General Electric Low Speed Research Compressor (LSRC) facility, described in more detail in Volume II (Reference 2), was used for this test program. The LSRC configuration, shown schematically in Figure 1, was a four-stage compressor having a constant casing diameter of 1.524 m (60 in) and a radius ratio of 0.85. A detailed cross section of one stage of the 0.85 radius ratio LSRC test vehicle is shown in Figure 2. The airfoils are 11.43 cm (4.5 in.) in span and approximately 9 cm (3.5 in.) in chord, large enough that blade edge and surface contours can be closely controlled during manufacture. The blades and vanes are constructed of inexpensive plastic materials and are molded in high pressure dies so that outstanding uniformity is achieved. The blades are hydraulically smooth at the test Reynolds number based on tip speed and blade chord of 360,000. Reynolds numbers of this magnitude are high enough to be above the critical value for compressor stages and, therefore, can provide a reasonable simulation of the performance of high-speed compressors.

The average rotor tip clearance-to-blade-height was 1.36 percent and the average stator seal clearance-to-blade-height was 0.78 percent. Circumferential groove casing treatment was applied over the tip of only the first rotor to assure that Stage 1 would not be the stall limiting blading.

3.2 TEST STAGES

Three alternate rear stage blading designs, Rotor B, Stator B, and Stator C, were tested in the present Screening Phase of the test program. These designs are described in detail in the Design Report (Reference 1) and are summarized in the following.

Rotor B was designed to the same set of vector diagrams as Rotor A but uses a type of meanline in the tip region that unloads the leading edge and loads the trailing edge relative to Rotor A. Previous test results had indicated that very small rotor wakes are present in the tip region of rotors similar in design to Rotor A. This region, therefore, should be able to take higher trailing edge loading without undue risk of separation. The modification to the tip region of Rotor B was blended into the pitchline so that Rotor A and Rotor B are identical from the pitchline to the hub. A photograph of Rotor B and a comparison of the Rotor A and B airfoil sections at the tip are given in Figure 3.

Stator B embodies blade sections twisted closed locally in the endwall regions similar to those used in a highly loaded NASA single stage that had rather good performance for its loading level (Reference 5). Different vector diagrams were calculated to account for the high values of swirl angle near

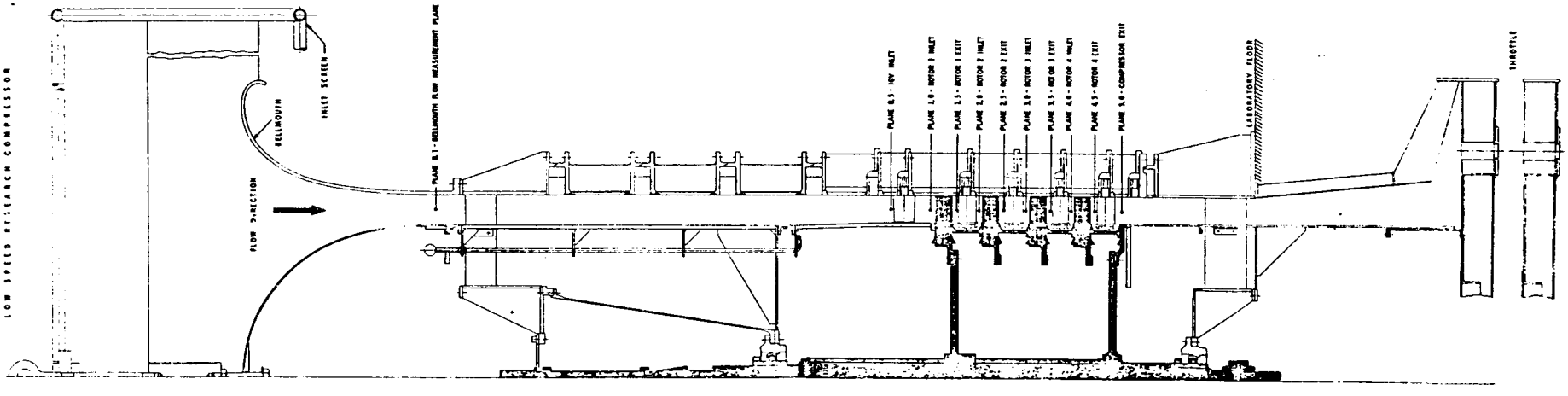

Figure 1. Four-Stage Compressor Configuration Tested in the NASA-GE Core Compressor Exit Stage Study.

FOLDOUT FRAME 2

FOLDOUT FRAME 1

FIGS 4 INTENTIONALLY BLANK

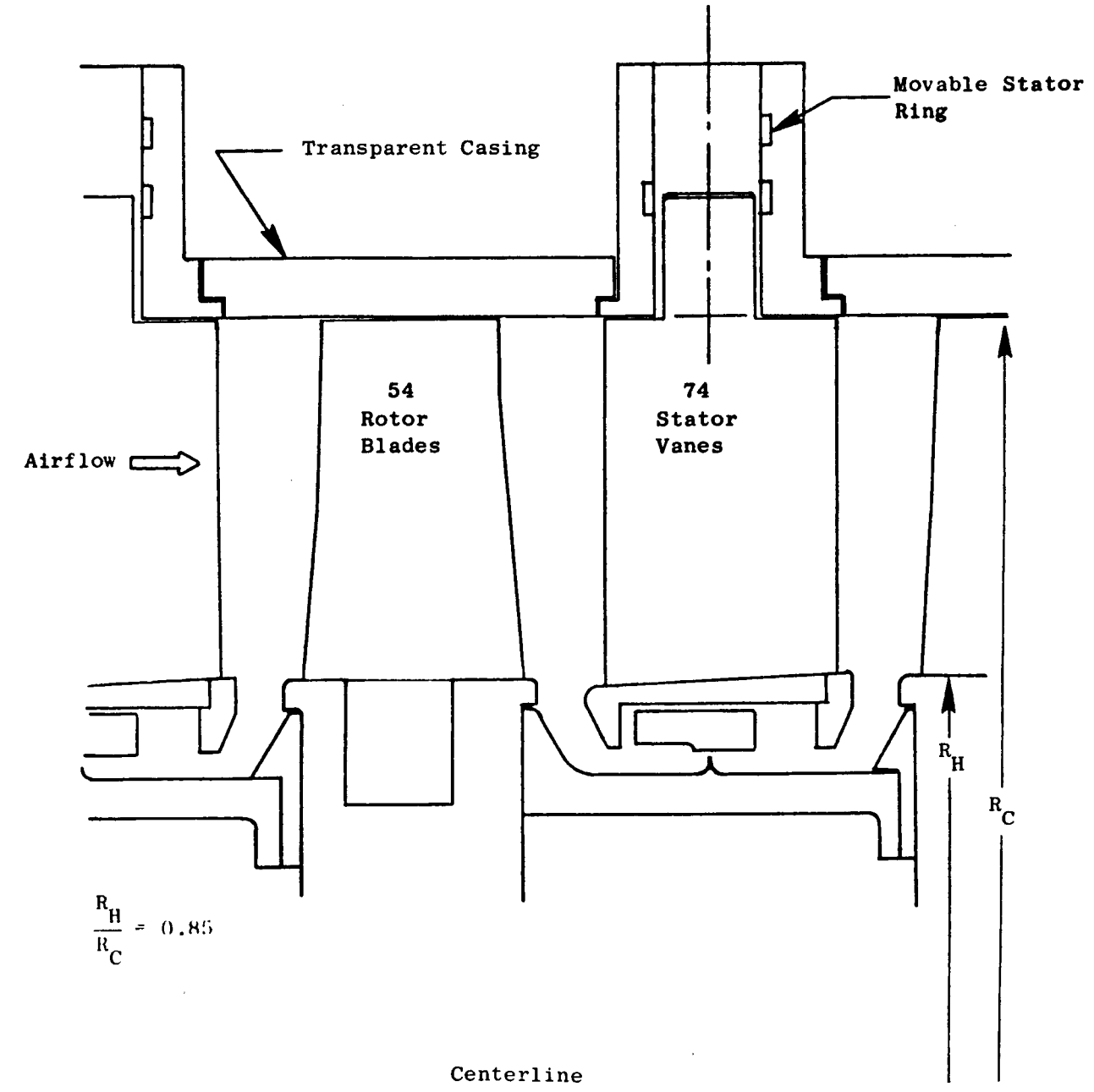

Figure 2. Cross Section of 0.85 Radius Ratio.

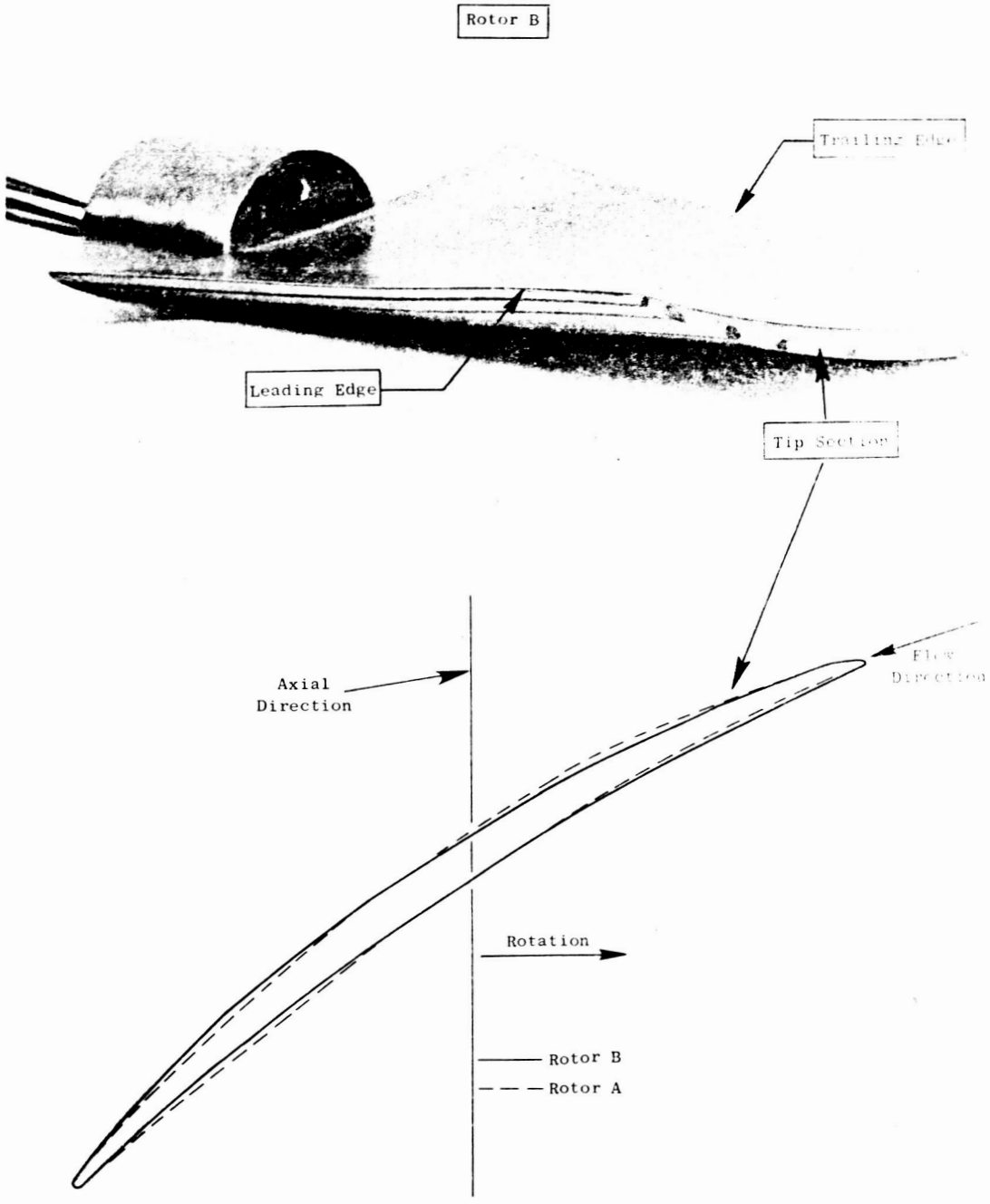

Figure 3. Photograph of Rotor B and Comparison of Rotor A and B Tip Sections.

the endwalls. The appearance of Stator B is quite different from that of Stator A because twist gradients were incorporated and because the vane was stacked at 30 percent chord from the leading edge in order to reduce the leading edge lean angle. A photograph of Stator B is shown in Figure 4.

Stator C embodies airfoil sections near the endwalls that have reduced trailing edge loading and increased leading edge loading relative to Stator A. The airfoils were designed to the same vector diagrams as Stator A. A photograph of Stator C and a comparison of Stator A and C airfoil sections are shown in Figure 5.

3.3 INSTRUMENTATION

The instrumentation used at various locations in the compressor for this screening test series is presented in Table 1. Standard total pressure rakes and wall static pressure taps were used. In addition, static pressure taps located on the blade and vane surfaces were used to determine the distribution of static pressure on the suction and pressure surfaces. Blades instrumented to yield this data are shown in Figures 3-6. In Figure 6 the blades are sealed on the pressure side at the hub so that no flow can leak from the pressure surface to the suction surface. The location of the surface static taps is given in Table 2. For rotors, the pressures are read by a pressure transducer/slip ring device.

The data recording and analysis procedures are automated. Pressures are measured using Bell and Howell Model No. 09384 low-pressure-range transducers having an accuracy of ±0.025% of the full-scale (12.44 kPA, 50 in. H_2O) reading. The data is automatically recorded in a time-sharing computer data file by an automated data controller.

More details about the instrumentation are given in Volume II (Reference 2).

3.4 TEST PROCEDURE

The overall test program was divided into four parts as outlined in Table 3. The first part involved extensive testing of the baseline blading, Stage A (Rotor A/Stator A), in both four-stage and single-stage configurations. The test results can be found in Volume II (Reference 2) of this series. The second part involved a series of short screening tests to select the best rotor design and the best stator design based upon tests in four-stage configurations. These test results are the subject of the present report. The third part involved extensive testing of the best rotor and best stator designs in combination using a four-stage compressor configuration. The test results can be found in Volume III. The final part of the test program will consist of extensive testing of a new Rotor C design in a four-stage configuration with Stator B, and the test results will be reported in Volume IV.

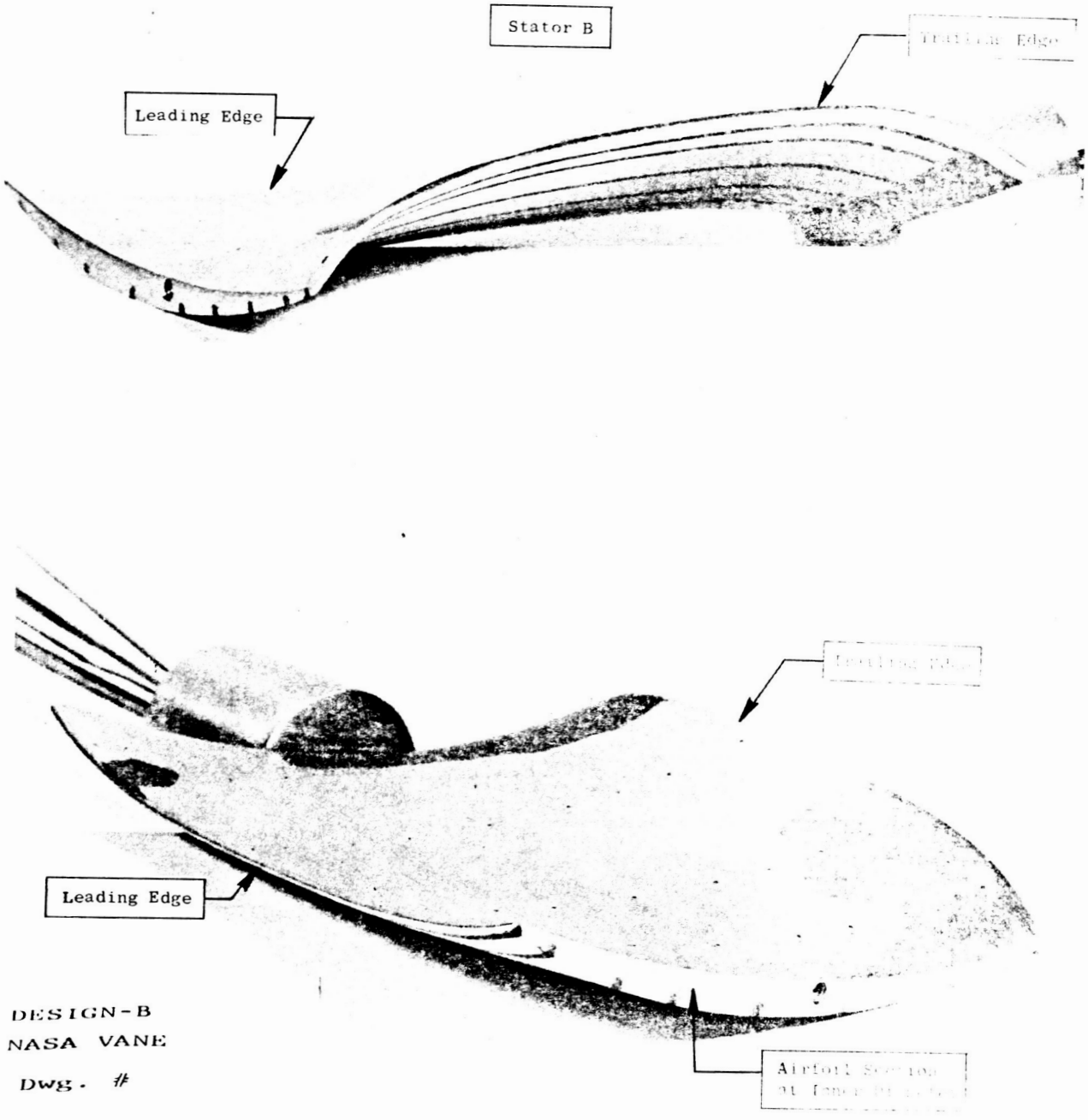

Figure 4. Photographs of Stator B.

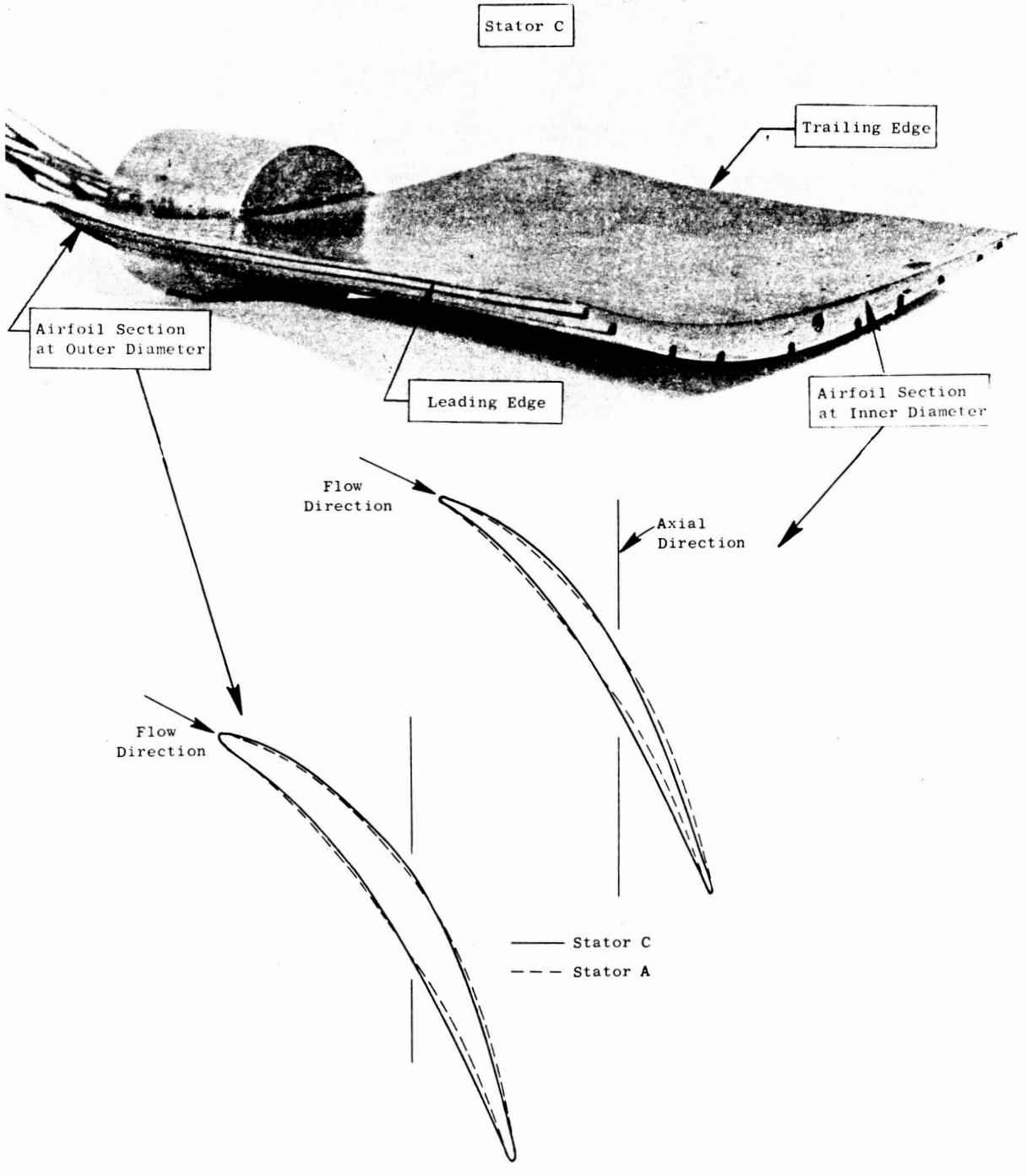

Figure 5. Photograph of Stator C and Comparison of Stator A and C Airfoil Sections.

Table 1. Instrumentation for the Screening Test.

Instrumentation	Plane Location										
	0.1 Bellmouth	0.5 IGV Inlet	1.0 R1 Inlet	1.5 S1 Inlet	2.0 R2 Inlet	2.5 S2 Inlet	3.0 R3 Inlet	3.5 S3 Inlet	4.0 R4 Inlet	4.5 S4 Inlet	5.0 Compressor Discharge
Static Pressure											
1. Casing Statics 11 Equally-Spaced Taps	X	X	X	X	X	X	X	X	X	X	X
2. Hub Statics 11 Equally-Spaced Taps	X	X	X								X
3. Hub Seal Cavity Static Pressures				X	X	X	X	X	X	X	
4. Single Element Traverse Probe*											
5. Blade or Vane Surface Static Pressure Taps							R3	S3			
Total Pressure											
1. 11 Element Radial Rake			X				X	X	X		X
2. Single Element Traverse Probe*							X	X	X		
3. Rotating Radial Rake								X			
Flow Angle											
1. Single Element Traverse Probe*											
Hot Film Probe*											

*Provisions for this instrumentation have been made at the planes indicated. However, the instrumentation was not in place for the screening tests.

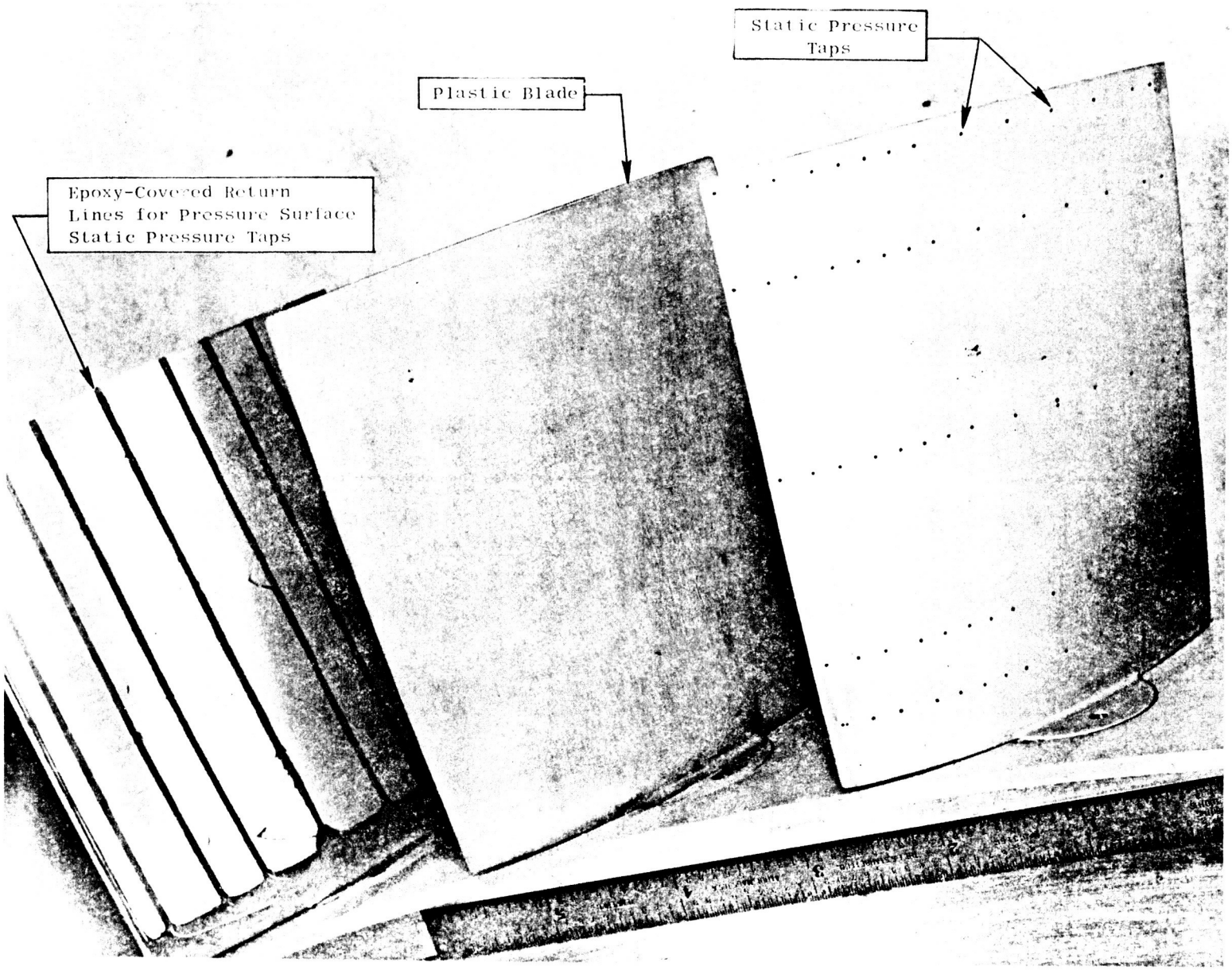

Figure 6. Rotor Blade with Static Pressure Taps on Suction Surface.

Table 2. Location of Surface Static Pressure Taps on Instrumented Airfoils.

Rotor

Suction Surface Tap Number	Percent Chord (%)	Distance From L.E. cm (in.)	Pressure Surface Tap Number	Percent Chord (%)	Distance From L.E. cm (in.)
1	2.5	0.229 (0.090)	1	2.5	0.229 (0.090)
2	8.0	0.726 (0.286)	2	8.0	0.726 (0.286)
3	13.0	1.184 (0.466)	3	20.0	1.821 (0.717)
4	20.0	1.821 (0.717)	4	30.0	2.733 (1.076)
5	25.0	2.276 (0.896)	5	45.0	4.100 (1.614)
6	30.0	2.733 (1.076)	6	60.0	5.466 (2.152)
7	35.0	3.188 (1.255)	7	70.0	6.375 (2.510)
8	40.0	3.642 (1.434)	8	80.0	7.287 (2.869)
9	50.0	4.554 (1.793)	9	90.0	8.199 (3.228)
10	60.0	5.466 (2.152)	10	95.0	8.654 (3.407)
11	70.0	6.375 (2.510)			
12	80.0	7.287 (2.869)			
13	90.0	8.199 (3.228)			
14	95.0	8.654 (3.407)			

Stator

Suction Surface Tap Number	Percent Chord (%)	Distance From L.E. cm (in.)	Pressure Surface Tap Number	Percent Chord (%)	Distance From L.E. cm (in.)
1	2.5	0.198 (0.078)	1	2.5	0.198 (0.078)
2	8.0	0.632 (0.249)	2	8.0	0.632 (0.249)
3	13.0	1.029 (0.405)	3	20.0	1.580 (0.622)
4	20.0	1.580 (0.622)	4	30.0	2.372 (0.934)
5	25.0	1.979 (0.779)	5	45.0	3.556 (1.400)
6	30.0	2.372 (0.934)	6	60.0	4.745 (1.868)
7	35.0	2.766 (1.089)	7	70.0	5.535 (2.179)
8	40.0	3.162 (1.245)	8	80.0	6.327 (2.491)
9	50.0	3.955 (1.557)	9	90.0	7.117 (2.802)
10	60.0	4.745 (1.868)	10	95.0	7.513 (2.958)
11	70.0	5.535 (2.179)			
12	80.0	6.327 (2.491)			
13	90.0	7.117 (2.802)			
14	95.0	7.513 (2.958)			

Radial Location of Pressure Taps

Rotor Immersion cm (in.) from Casing	Rotor Percent Immersion from Casing (%)	Stator Immersion cm (in.) from Casing	Stator Percent Immersion from Casing (%)
0.572 (0.225)	5	1.143 (0.450)	10
2.286 (0.900)	20	2.286 (0.900)	20
5.715 (2.250)	50	5.715 (2.250)	50
9.144 (3.600)	80	9.144 (3.600)	80
10.287 (4.050)	90	10.859 (4.275)	95

Table 3. Overall Test Plan Outline for Complete Program.

I. Tests using Stage A Blading (Reported in Ref. 1)	
A. Shakedown Test	5 data points
B. 4-Stage Configuration (Third Stage as Test Stage)	
1. Preview Data	15 data points
2. Stall Determination	As appropriate
3. Casing Treatment Data	15 data points
4. Reynolds Number Data	30 data points
5. Standard Data	4 data points
6. Blade Element Data	4 data points
7. Blade Surface Pressure Data	2 data points
8. Detailed Wall Boundary Layer Data	2 data points
C. 1-Stage Configuration	
1. Preview Data	15 data points
2. Stall Determination	As appropriate
3. Standard Data	4 data points
4. Blade Element Data	4 data points
5. Blade Surface Pressure Data	4 data points
6. Detailed Wall Boundary Layer Data	2 data points
D. 4-Stage Configuration (First Stage as Test Stage)	
1. Blade Element Data	4 data points
2. Blade Surface Pressure Data	4 data points
3. Detailed Wall Boundary Layer Data	2 data points
II. Screening Tests	
A. 4-Stage Configuration with Rotor B and Stator A	
1. Preview Data	15 data points
2. Stall Determination	As appropriate
3. Standard Data	4 data points
4. Blade Surface Pressure Data	4 data points
B. 4-Stage Configuration with Stator B and Rotor A	
(Same Data as II.A.)	
C. 4-Stage Configuration with Stator C and Rotor A	
(Same Data as II.A.)	
D. 4-Stage Configuration with Rotor B and Stator B	
(Same Data as II.A.)	
III. Tests Using Rotor B and Stator B Designs (4-Stage Configuration, Third Stage as Test Stage)	
1. Same Data as I.B	
2. Rotor Tip Clearance Data	
IV. Tests Using Rotor C and Stator B Designs	
(4-Stage Configuration, Third Stage as Test Stage)	
1. Same Data as I.B	

The major intent of the screening tests was to evaluate quickly each rotor and stator design in a systematic fashion in order to select the best blading designs. All of the screening tests were conducted using a four-stage configuration. Rotor B was tested with Stator A to determine the better rotor. Then Stator B was tested with Rotor A, and Stator C was tested with Rotor A to determine the best stator. The best rotor, Rotor B, and the best stator, Stator B, were then tested in a four-stage configuration.

Four types of data were taken during the Screening Tests: Preview Data, Stall Determination Data, Standard Data and Blade and Vane Surface Pressure Data. A brief description of each of these types of data is presented in the following. Preview Data provides stage characteristics and efficiency measurements based on casing static pressure rise from Rotor 1 inlet to Stator 4 exit, measured airflow and measured torque. Stall Determination Data consists of observing the sudden decrease in the static pressure rise across the compressor at stall and of listening for the onset of rotating stall. Standard Data provides performance based on mass-averaged total pressure rise from Rotor 1 inlet to Stator 4 exit. Blade and Vane Surface Pressure Data provide a means of determining regions of favorable incidence angle, rates of diffusion, and regions of separated flow on the airfoil.

Evaluation and comparison for all of these data from the various configurations have provided a means of assessing the effectiveness of the particular design approaches employed for reducing endwall region losses.

3.5 DATA REDUCTION AND ANALYSIS METHODS

The data analysis procedures to be followed in reducing test data have been described in Volume II (Reference 2) of the report. Additional discussion of the data reduction method for Blade Surface Pressure Data is presented in the following.

Theoretical velocity distributions along the suction and pressure surfaces of the blades and vanes in the Low Speed Research Compressor were computed by using the Cascade Analysis by Streamline Curvature (CASC) computer program as discussed in Reference 1 for operation near the design point. In order to compare these CASC distributions with experimentally measured distributions, one must calculate the velocities on the blade and vane surfaces from the static pressures measured on these surfaces. The equation which relates the normalized velocities and the measured pressures is

$$\frac{V}{V_1} = \left(\frac{P_{T_1} - P_S}{P_{T_1} - P_{S_1}} \right)^{\frac{1}{2}} F_c \qquad (1)$$

where the non-subscripted variables indicate blade surface conditions, the Subscript 1 indicates upstream conditions, F_c is a compressibility correction (which was taken as unity since the Mach number was so low), and total pressure is assumed constant. For each radial immersion where comparisons were made, the blade surface static pressures, P_S, were obtained from experimental measurements. However, the upstream static pressure, P_{S_1}, and the total pressure, P_{T_1}, required for Equation 1 were not measured at interstage locations as part of the Screening Test procedure because of the complexities of obtaining such measurements.

The upstream static pressure was obtained from radial distributions of static pressure determined as follows. The circumferential-average casing static pressure was measured at Planes 3.0 and 3.5 (Table 1) as part of Standard Data in the Screening Test series. This value of casing static pressure at either Plane 3.0 for Rotor 3 or Plane 3.5 for Stator 3 at the design point served as an anchor for a generalized profile of the radial variation of static pressure which was measured previously as part of the comprehensive tests of the Rotor A/Stator A Configuration described in Reference 2.

The total pressure used in Equation 1 to calculate velocity ratios for each airfoil section was taken to be that value of total pressure which made the minimum velocity ratio on the pressure surface as computed from the measured data equal to the minimum velocity ratio on the pressure surface as computed by CASC. Although this technique for obtaining total pressure does not provide valid comparisons of velocity magnitude between the CASC results and the experimental results, it does provide comparisons of the shape of surface velocity distributions that are useful in diagnosing differences in incidence angle and regions of flow separation.

4.0 RESULTS AND DISCUSSION

Screening Test results have been obtained for the rear stage blading designs that were developed to have lower losses in their endwall boundary layer regions. The results are presented in the following.

4.1 OVERALL PERFORMANCE

The overall performance of each Screening Test configuration was determined from Preview Data and Standard Data. These test data are presented as graphs of pressure coefficient, work coefficient and torque efficiency plotted as a function of flow coefficient. All tests were conducted using a four-stage configuration having an average rotor tip clearance-to-blade-height of 1.36 percent and an average stator seal clearance-to-blade-height of 0.78 percent. The tests were conducted at a Reynolds number of 3.6×10^5. As discussed in Reference 2, circumferential groove casing treatment was applied over the tip of only the first rotor to assure that Stage 1 would not be the stall limiting blading.

Rotor B with Stator A

The performance of Rotor B, which has a tip region design that unloads the leading edge and loads the trailing edge relative to Rotor A, is compared to the performance of the baseline Rotor A in Figure 7. Rotor B and Rotor A are both running with Stator A. The important feature of this performance comparison is the 0.3 point improvement in efficiency obtained at the design point and at higher flows with Rotor B. However, since measurements of rotor loss were not made, the implication that Rotor B has lower tip losses than Rotor A can be only surmised at this time. The pressure/flow characteristic of the two rotors is similar, but Rotor B has a slight increase in pumping and a 7.3 percent increase in stall airflow. The slight increase in pumping may be related to slight unintended differences in blade geometry or blade setting angles. The decrease in flow range of Rotor B compared with Rotor A may be due to the new airfoil shape in the tip section or to slight unintended differences in tip clearance since abrupt stall is thought to originate in the tip region. This decrease in stall flow is not considered to be too significant since the range from the design point to the peak pressure rise point is virtually unchanged from the baseline and since rear stages of this type will probably not operate beyond the peak pressure rise point in a high-speed compressor.

The radial variation of normalized total pressure at the compressor discharge is presented in Figure 8 for the design point throttle, the peak efficiency throttle and the peak pressure rise throttle for all of the screening test configurations. Although there is a difference in pressure level between the Rotor B/Stator A configuration and the Rotor A/Stator A configuration, the

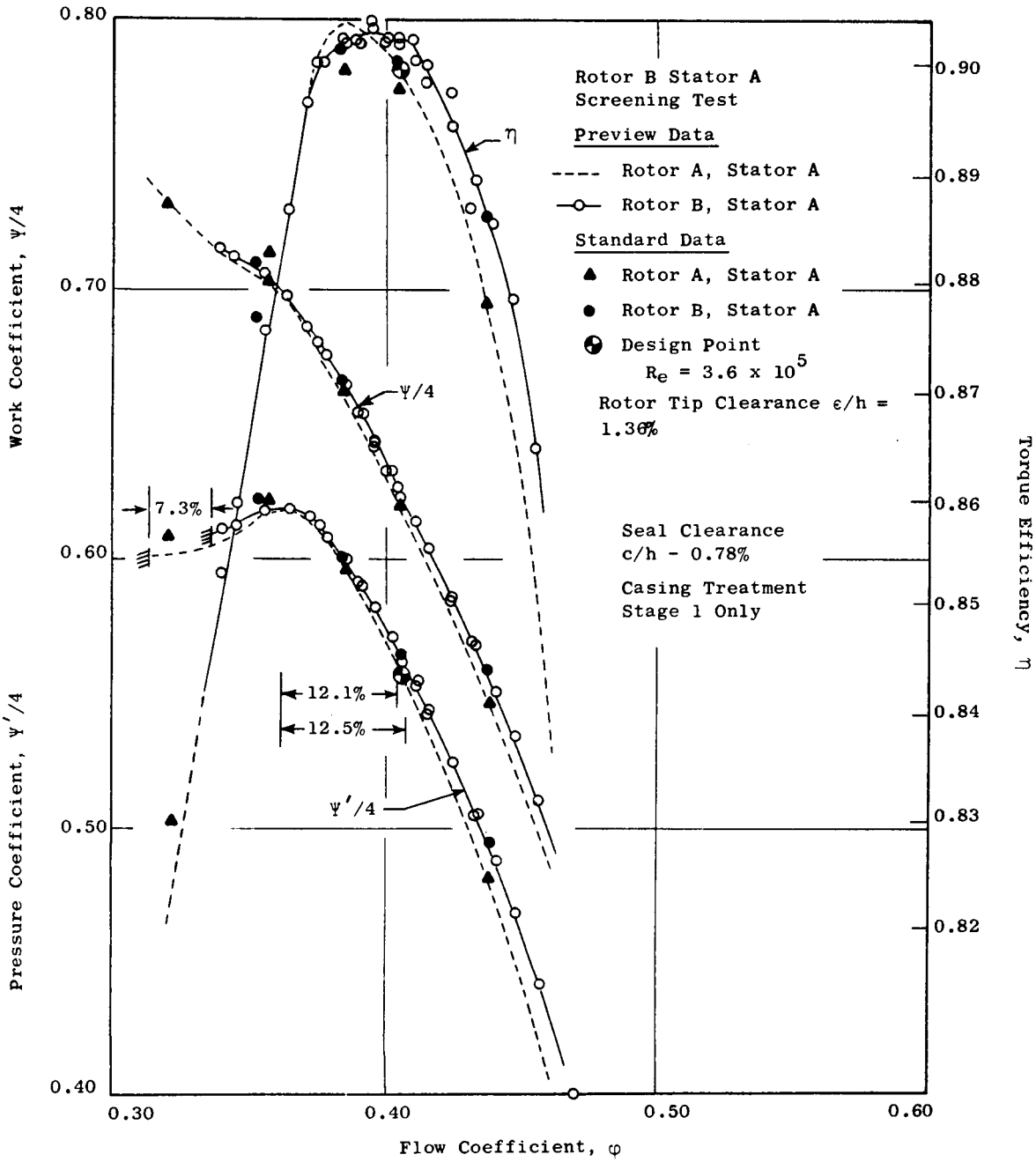

Figure 7. Comparison of the Overall Performance of Rotor B and Rotor A, Both are Four-Stage Configurations Running with Stator A.

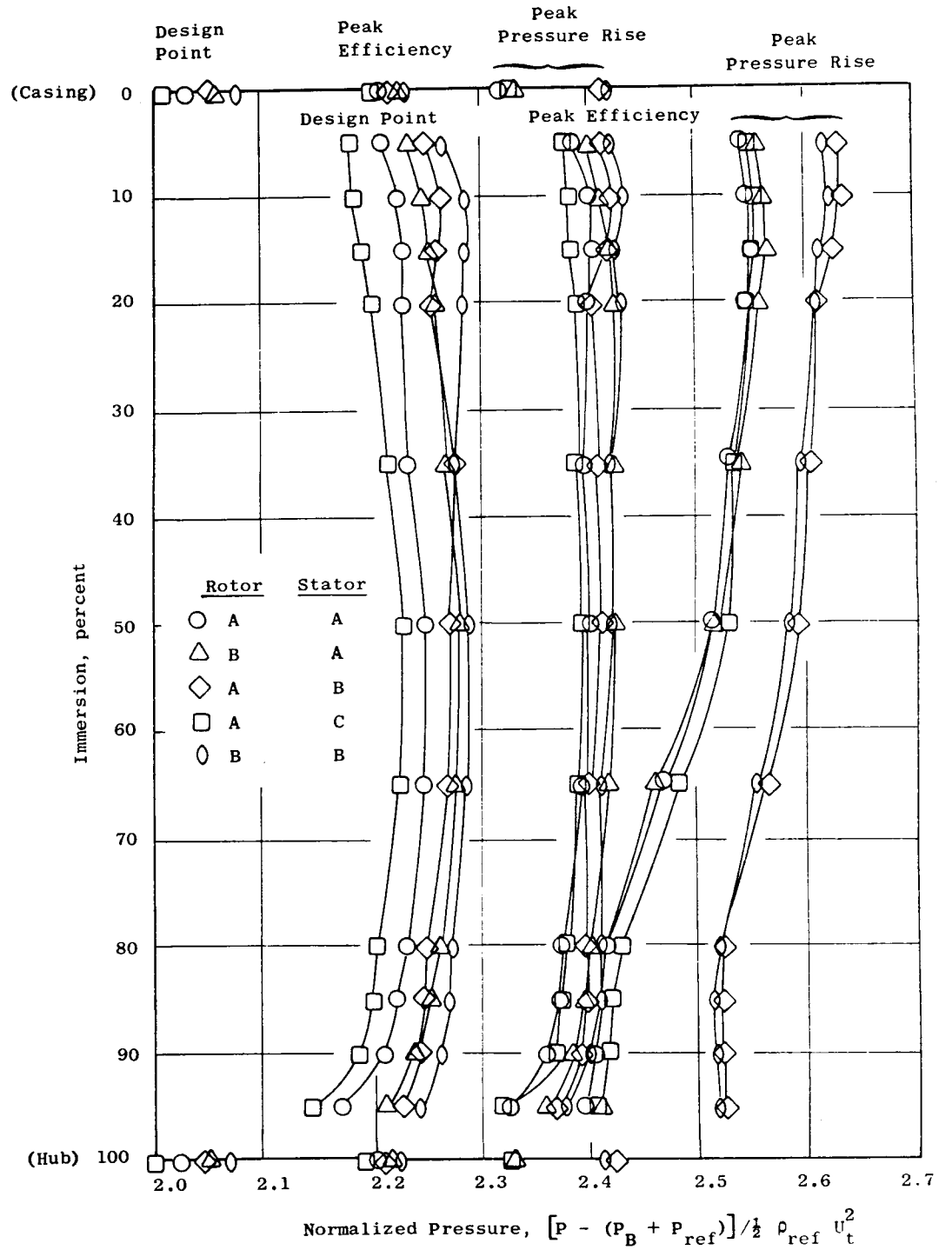

Figure 8. Radial Variation of Normalized Total Pressure Including Casing and Hub Normalized Static Pressures at the Compressor Discharge for Various Throttle Settings.

shape of the radial distribution at each throttle is very similar. Of particular significance in Figure 8 is the weakening and eventual collapse of the hub region at peak pressure rise for both the Rotor B/Stator A and the Rotor A/Stator A configurations. From 80 percent immersion to the hub, very little total pressure rise has been achieved as the Rotor B/Stator A configuration is throttled from peak efficiency to peak pressure rise. Boundary separation at the hub is occurring and becoming progressively worse as stall is approached. This results in the rollover and flattening of the pressure-flow characteristic from peak pressure rise to stall in Figure 7.

Stator B with Rotor A

The performance of Stator B, which embodies twist gradients in the endwall regions, is compared to the performance of the baseline Stator A in Figure 9. Stator B and Stator A are both running with Rotor A. Two important features of this performance comparison are: (1) an improvement in efficiency at every flow tested using Stator B with a 0.4 to 0.5 point improvement obtained at the design point and (2) a significant improvement in the pressure-flow characteristic obtained near stall using Stator B. The 3.2 percent improvement in peak pressure coefficient and the 5.4 percent improvement in flow range from the design point to the peak pressure rise point result, in part, from more favorable airfoil pressure distributions, especially near the hub, as will be shown later.

The six percent increase in stalling flow coefficient for Stator B is not thought to be too significant, especially in view of the 5.4 percent improvement in flow range from design to peak pressure rise, since rear stages of this type will probably not operate beyond the peak pressure rise point in a high-speed compressor. Also there is a very slight increase in pumping for the Rotor A/Stator B configuration.

The radial variation of normalized total pressure at the compressor discharge was presented in Figure 8. Although the shapes of the radial distributions for the Rotor A/Stator B configuration at design and peak efficiency are rather similar to those for the Rotor A/Stator A configuration, the use of Stator B has produced a significant strengthening of the hub region at peak pressure rise. This results in the improvement of the pressure-flow characteristic for the Rotor A/Stator B configuration shown in Figure 9.

Stator C with Rotor A

The performance of Stator C, which has reduced trailing edge loading and increased leading edge loading near the endwalls, is compared to the performance of the baseline Stator A in Figure 10. Stator C and Stator A are both running with Rotor A. There is a 0.3 point loss in peak efficiency using Stator C. The slight loss in efficiency for Stator C at the design point is within experimental accuracy. Since Stator C shows no obvious advantages either in the performance shown in Figure 10 or in the radial variation of total pressure shown in Figure 8, no further testing of it is planned.

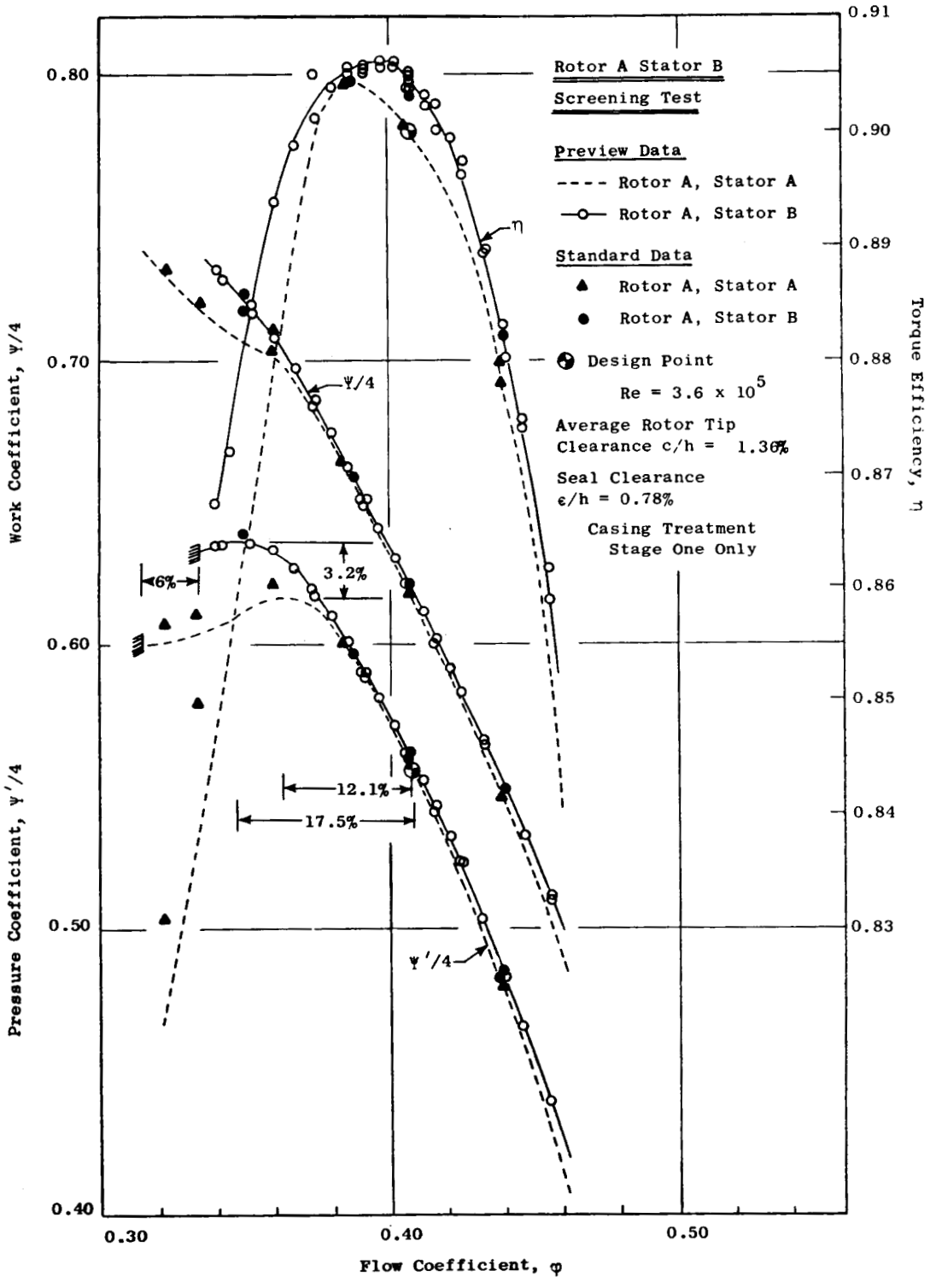

Figure 9. Comparison of the Performance of Stator B and Stator A; Both Are 4-Stage Configurations Running with Rotor A.

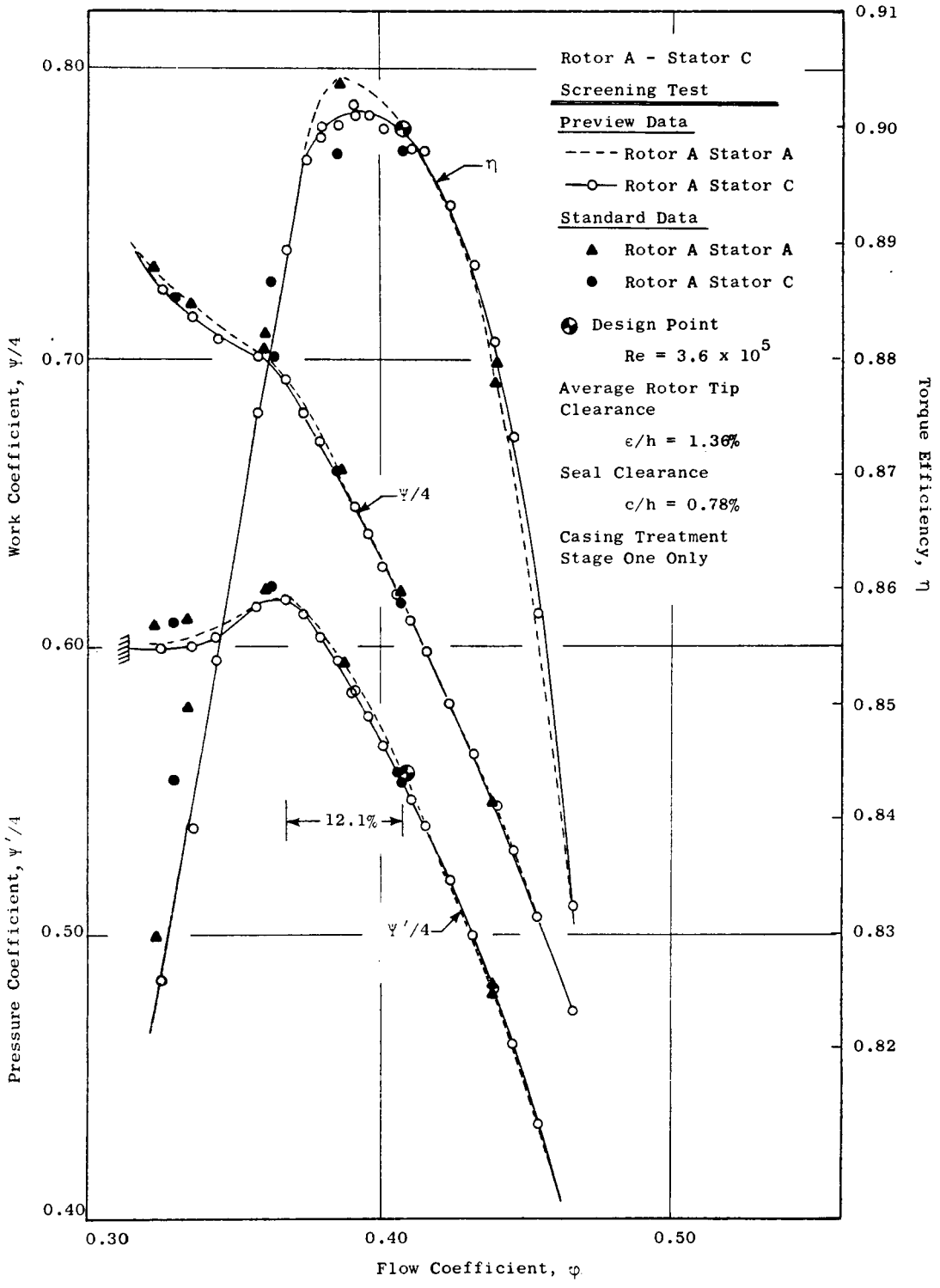

Figure 10. Comparison of the Performance of Stator C and Stator A, Both are Four-Stage Configurations Running with Rotor A.

Rotor B with Stator B

Since the Rotor B design and the Stator B design both showed a performance improvement when compared with the baseline, a four-stage configuration consisting of Rotor B/Stator B was tested in an effort to find the best stage. The performance of this configuration is compared to the performance of the baseline Rotor A/Stator A configuration and that of the Rotor A/Stator B configuration in Figure 11. Apparently, the gains achieved individually by Rotor B and Stator B are not additive. The performance of the Rotor B/Stator B configuration generally follows that of the Rotor A/Stator B configuration but with slightly higher efficiencies at flow rates larger than design flow and slightly lower efficiencies at flow rates smaller than design. When compared with the baseline, Rotor B/Stator B shows: (1) a 0.3 to 0.4 point improvement obtained at the design point and (2) a significant improvement in the pressure-flow characteristic near stall. The 2.8 percent improvement in peak pressure coefficient and the 5.4 percent improvement in flow range from the design point to the peak pressure point result from a more favorable pressure distribution on the airfoil, especially near the hub. The 5.4 percent improvement in flow range from design to peak pressure rise obtained with the Rotor A/Stator B configuration has been maintained.

The radial variation of normalized total pressure at the compressor discharge, shown in Figure 8, generally follows that of the Rotor A/Stator B configuration, indicating that the strengthening of the hub region at peak pressure rise has been maintained.

Based on these results, the Rotor B/Stator B configuration has been selected to undergo detailed testing in the next phase of the program.

4.2 STATIC PRESSURE MEASUREMENTS ON BLADE AND VANE SURFACES

The measurements of static pressure on the blade and vane surfaces are presented in Figures 12 through 21 for the various Screening Test configurations. The measured pressures have been normalized by the dynamic head based on tip speed, $1/2\ \rho_{ref}\ U_t^2$. Suction surface measurements are presented as solid lines and pressure surface measurements as dashed lines. Data were obtained for an open throttle, the design throttle, the peak efficiency throttle, the peak pressure rise throttle and the near stall throttle. In this section the discussion will concentrate on how loadings shift as the compressor is throttled. In Section 4.3, comparisons with design calculations will be presented.

Rotor B with Stator A

The normalized static pressure measurements on the blade and vane surfaces are presented in Figures 12 and 13 for the Rotor B/Stator A configuration.

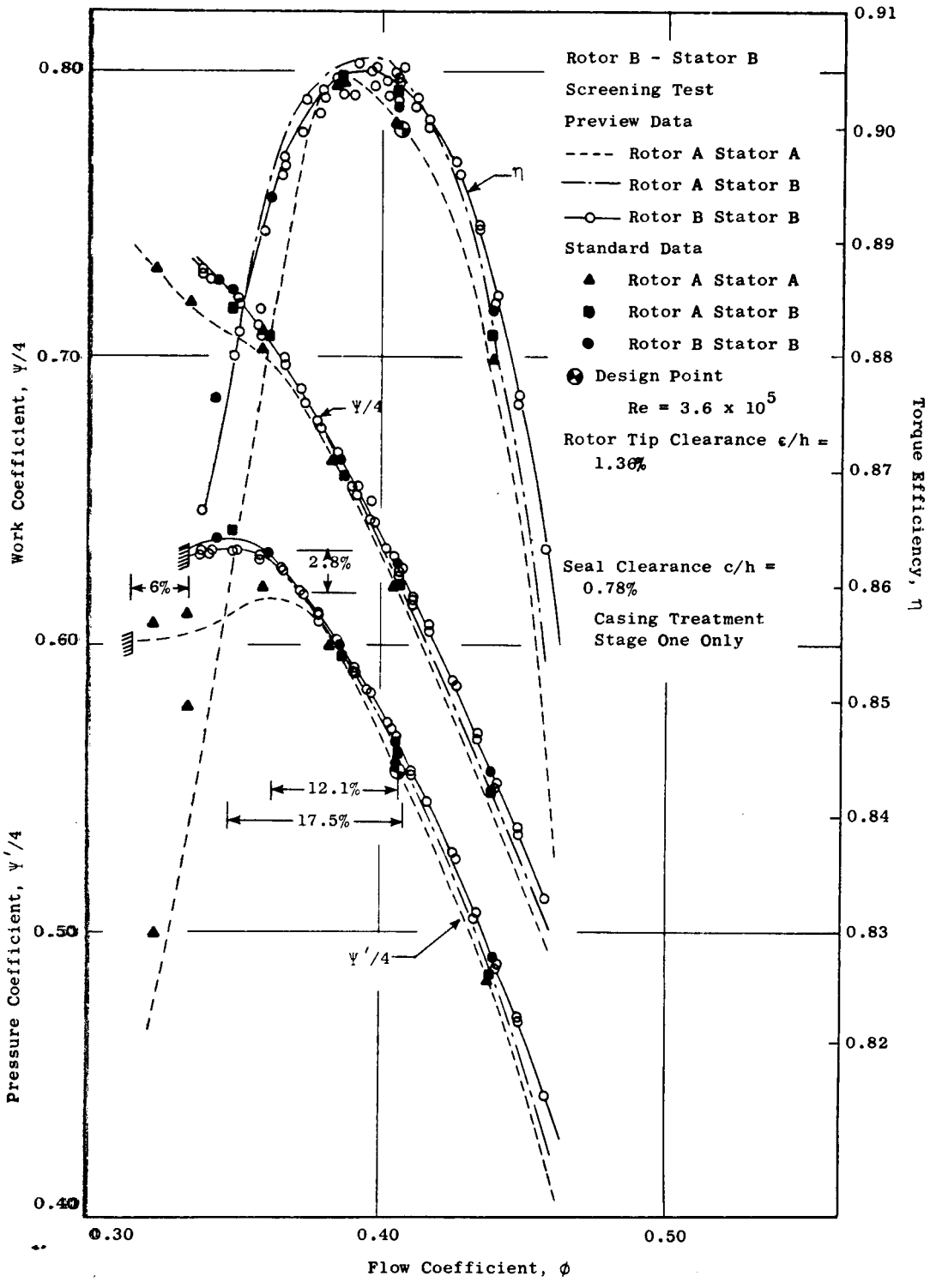

Figure 11. Rotor B/Stator B Performance.

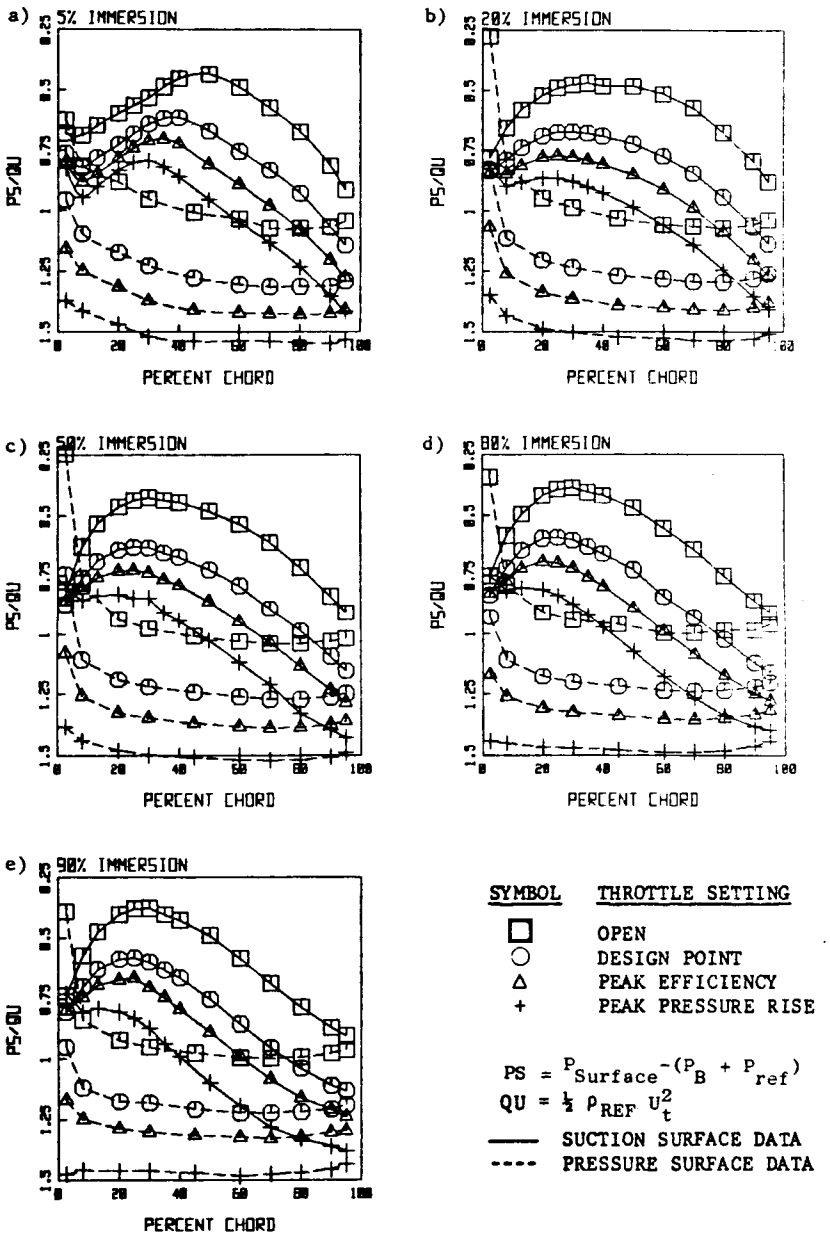

Figure 12. Rotor Blade Surface Static Pressure Measurements for the 4-Stage Rotor B/Stator A Configuration; Third Stage is Test Stage.

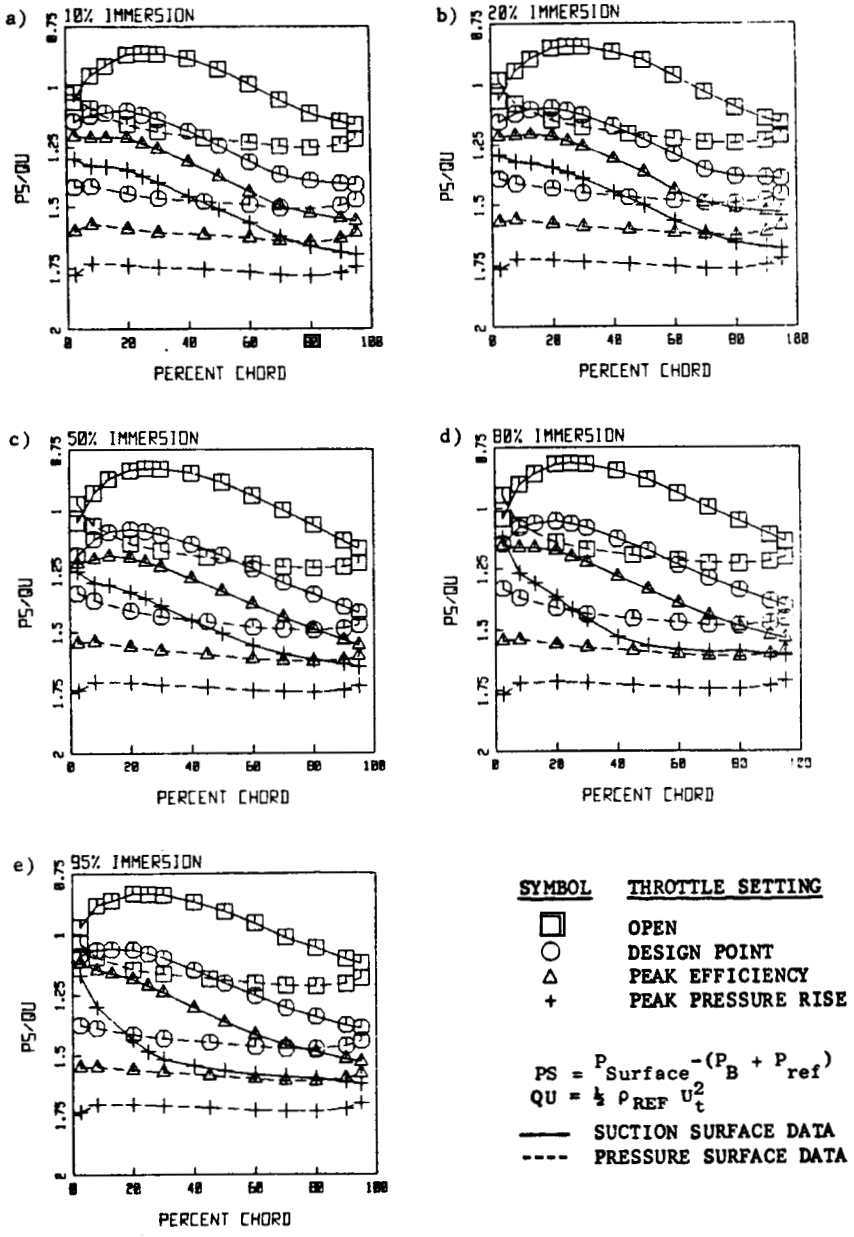

Figure 13. Stator Vane Surface Static Pressure Measurements for the 4-Stage Rotor B/Stator A Configuration; Third Stage is Test Stage.

The rotor data in Figure 12 indicate that the principal feature of Rotor B, its increased diffusion rate at the trailing edge near the tip, was successfully accomplished. The continuous diffusion from the location of the peak suction surface velocity (minimum static pressure) to the trailing edge for all blade sections from the pitchline to the tip and for all throttle settings indicates that the trailing edge region was able to take this increased aft loading without flow separation (Figure 12a, b, c). Evidence of flow separation near the hub can be seen in the distinct change in slope of the static pressure distribution on the suction surface at 70 percent chord for the peak pressure rise throttle (Figure 12e).

The increase in leading edge loading as the compressor is throttled toward stall is seen as a decrease in suction surface pressure and an increase in pressure surface pressure near the leading edge for all immersions. However, no large suction surface spike appears to form; this suggests that stall probably does not initiate because of excessive rotor incidence, although this is not certain.

There is evidence of the effects of secondary flow and tip leakage on the suction surface pressure distribution over the first 25 percent of chord (Figure 12a). This is seen as an increase in static pressure on the suction surface from zero to about eight percent chord followed by a decrease in static pressure from eight to about 40 percent chord. This same type of profile was observed on the suction surface near the tip in Reference 5 although the location of maximum static pressure occurred further aft.

The stator data in Figure 13 suggest that the diffusion pattern on the suction surface is not as healthy as that on the rotor. The rate of diffusion tends to decrease near the trailing edge indicating boundary layer separation may be developing. This flow separation on the suction surface becomes significantly more evident near the hub at the peak pressure rise throttle as seen in Figure 13d and 13e. For this case a significant flow separation has occurred between 30 and 40 percent chord, probably as a result of excessive incidence. Probing this region with a tuft-probe confirmed the presence of large areas of separated flow.

Stator B with Rotor A

The general characteristics of the Rotor A data in Figure 14 are similar to those of the Rotor B data in Figure 12, namely: (1) a continuous diffusion from the location of the peak suction surface velocity (minimum static pressure) to the trailing edge that gives little indication of flow separation until the peak pressure rise throttle near the hub (Figure 14e) and (2) evidence of the effects of secondary flow/tip leakage on the suction surface pressure distribution near the leading edge of the tip.

The stator data in Figure 15 indicate: (1) a Stator B leading edge loading that is slightly lower than that obtained for Stator A shown in Figure 13, and (2) a diffusion pattern on the suction surface of Stator B which is more

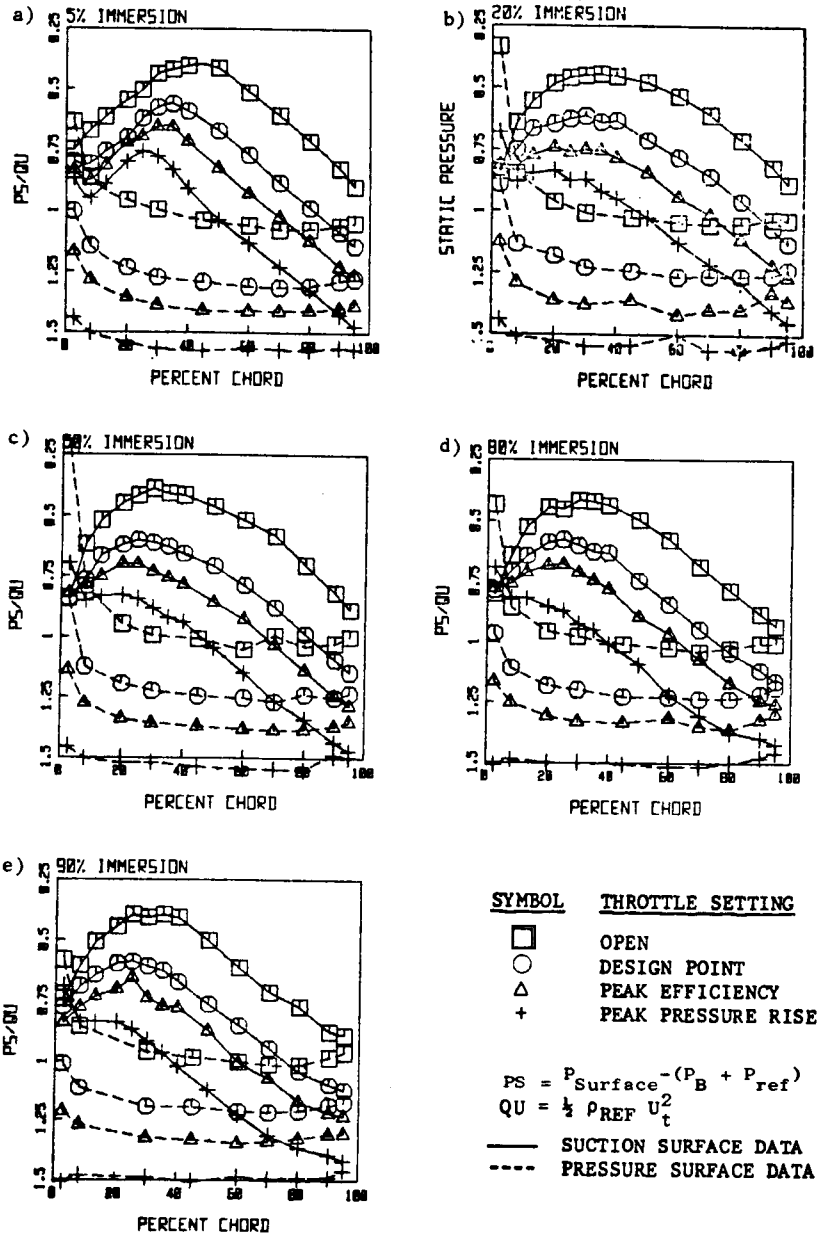

Figure 14. Rotor Blade Surface Static Pressure Measurements for the 4-Stage Rotor A/Stator B Configuration; Third Stage is Test Stage.

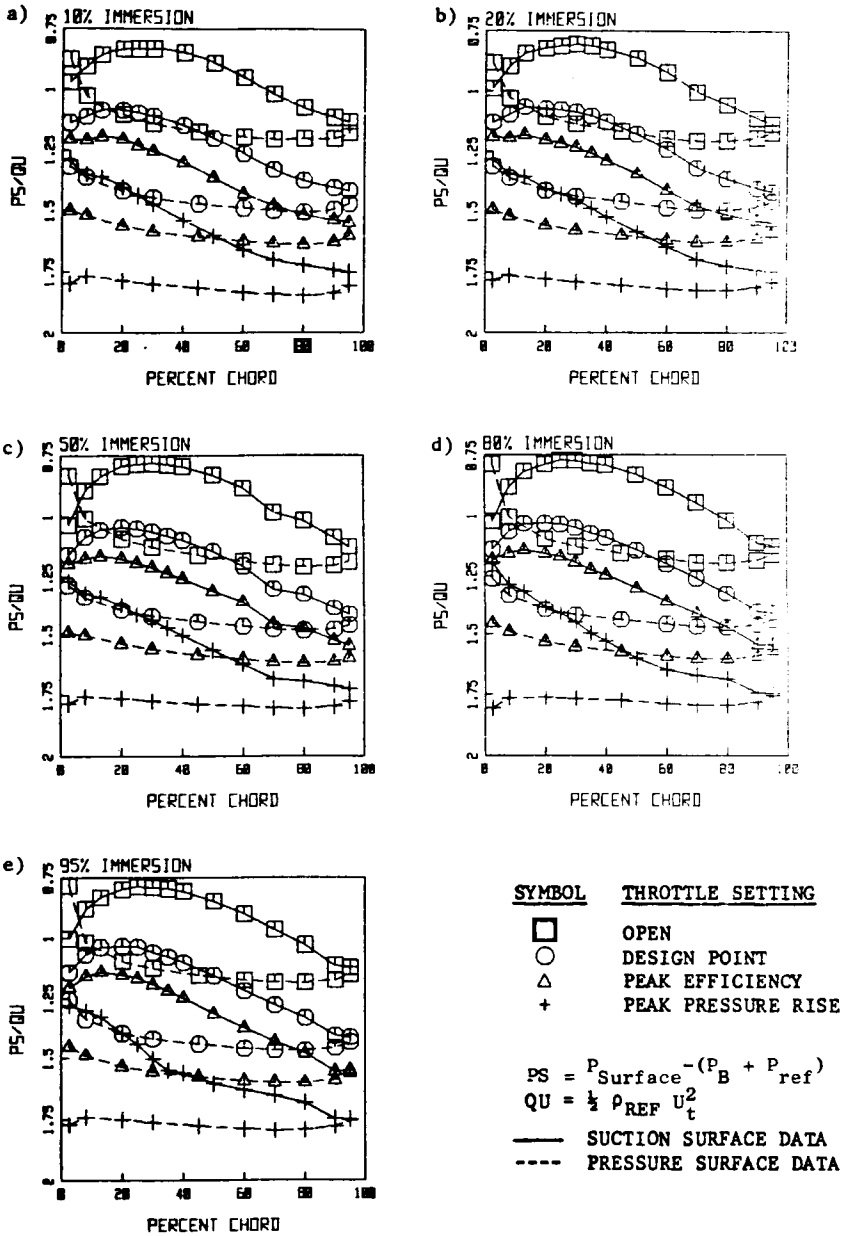

Figure 15. Stator Vane Surface Static Pressure Measurements for the 4-Stage Rotor A/Stator B Configuration; Third Stage is Test Stage.

favorable near the hub than that obtained for Stator A, although strong evidence of flow separation at the hub still exists for the peak pressure rise throttle (Figure 15d and 15e). The more favorable diffusion pattern obtained for Stator B can be seen by comparing Figures 15d and 15e with Figure 13d and 13e. This is especially evident at 95 percent immersion for the open throttle, the design throttle and the near-peak-efficiency throttle. This more favorable diffusion pattern would help to explain the increased efficiency at the design point and the significant improvement in the pressure-flow characteristic at lower flows shown in Figure 9.

Stator C with Rotor A

The rotor data in Figure 16 are similar to those obtained before for Rotor A and discussed in the previous section.

The diffusion patterns on the suction surface of Stator C in Figure 17 show no significant advantages over those obtained for the baseline Stator A. A large area of flow separation is still very apparent on the suction surface near the hub. Based upon this data, no further testing of Stator C was conducted.

Rotor B with Stator B

The normalized static pressure measurements on the blade and vane surfaces are presented in Figures 18 and 19 for the four-stage configuration consisting of the best rotor, Rotor B, and the best stator, Stator B. The surface pressure distributions for Rotor B and Stator B are virtually identical to those obtained for Rotor B and Stator A in the earlier tests reported in Figures 12 and 13 respectively. Consequently a discussion of these test results will not be repeated here.

The surface static pressure measurements for Rotor B are compared with those for Rotor A at five percent immersion in Figure 20. These data indicate that the Rotor B design intent of unloading the leading edge region and loading the trailing edge region relative to Rotor A has been achieved.

The surface static pressure measurements for Stator B are compared with those for Stator A at 95 percent immersion in Figure 21. These data suggest that Stator B is running at a more favorable (lower) incidence angle than Stator A and that Stator B has more diffusion than Stator A from 60 percent chord to the trailing edge. Evidence of flow separation does not appear for Stator B until about 90 percent chord. This would help to explain the performance improvement obtained with Stator B relative to Stator A shown in Figures 9 and 11.

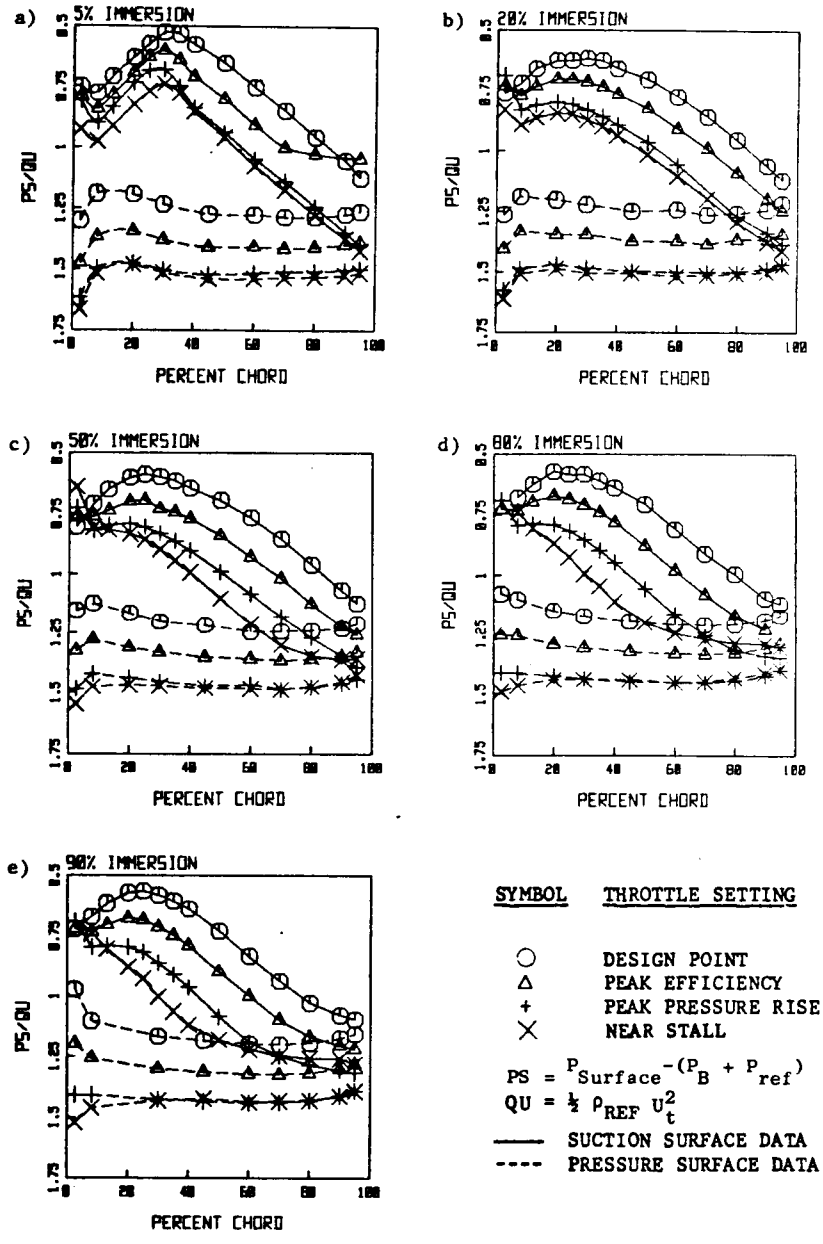

Figure 16. Rotor Blade Surface Static Pressure Measurements for the 4-Stage Rotor A/Stator C Configuration; Third Stage is Test Stage.

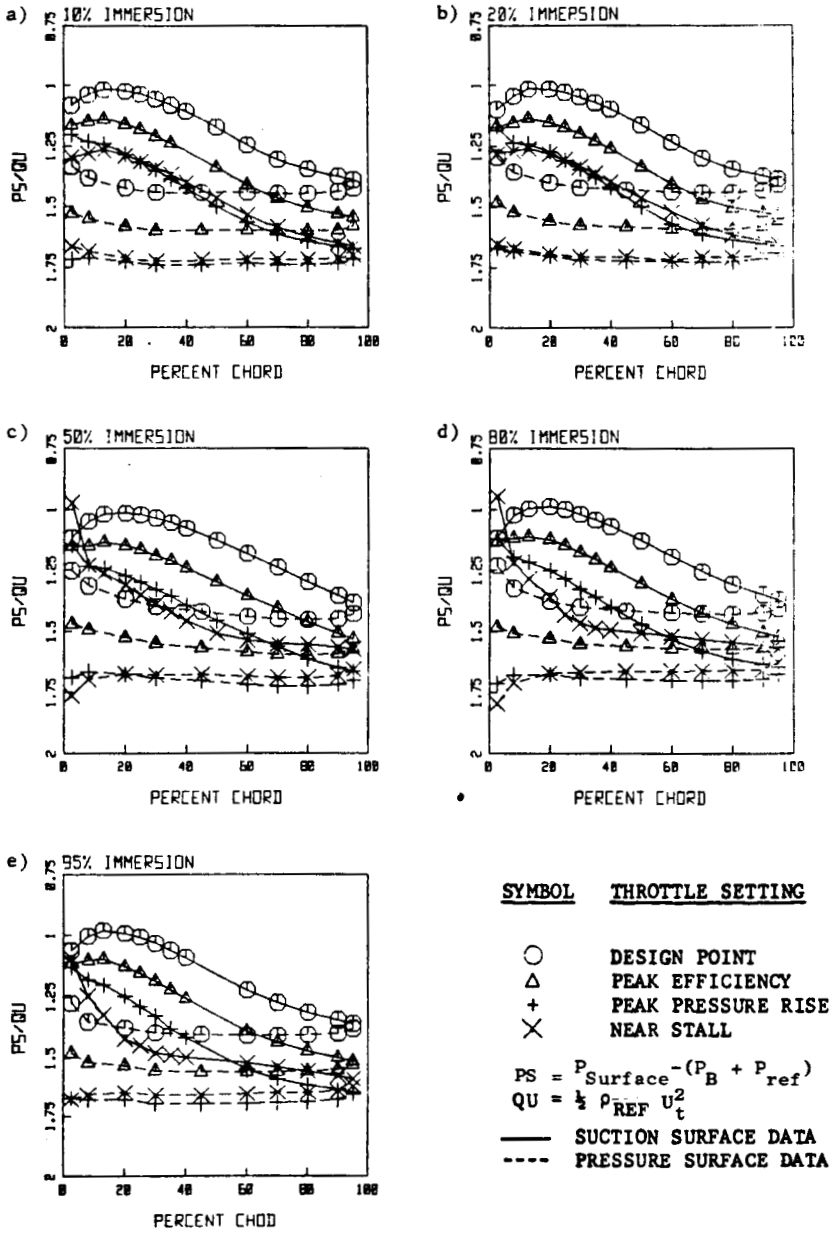

Figure 17. Stator Vane Surface Pressure Measurements for the 4-Stage Rotor A/Stator C Configuration; Third Stage is Test Stage.

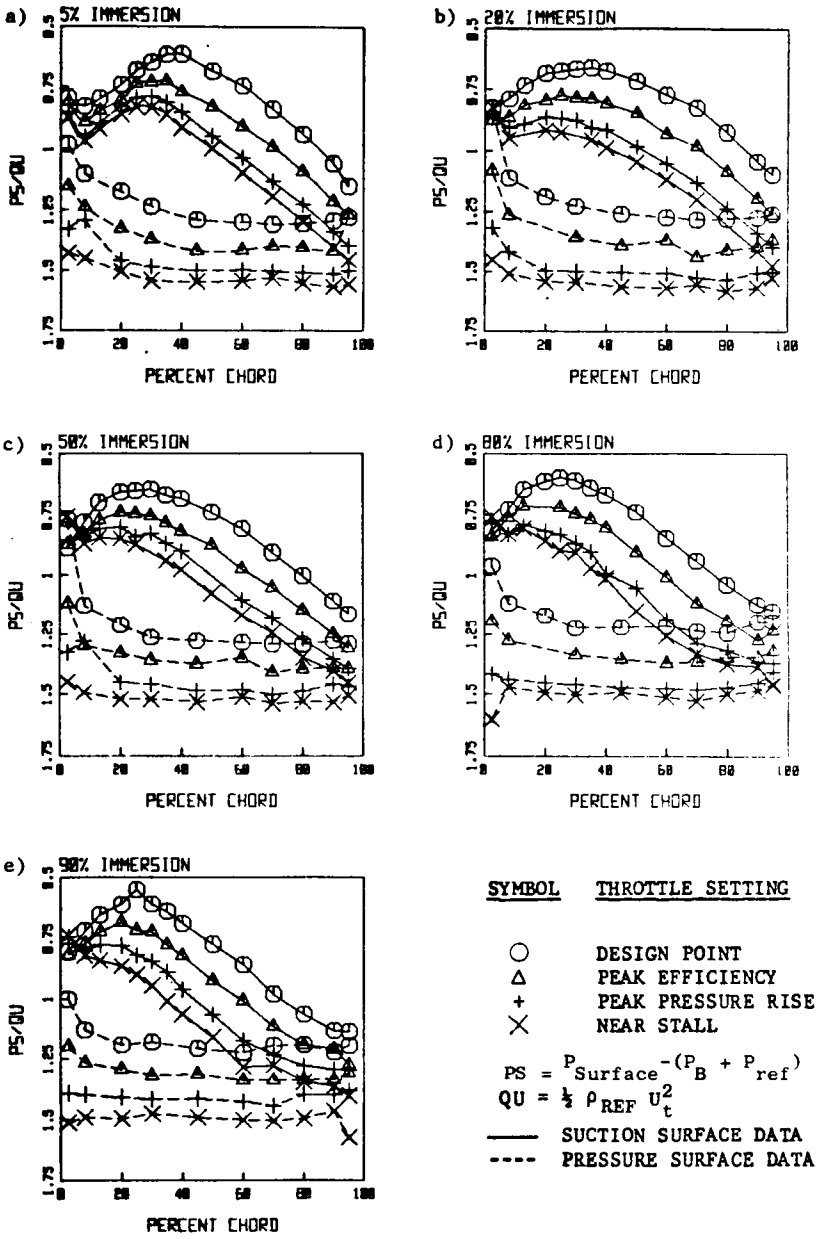

Figure 18. Rotor Surface Static Pressure Measurements for the 4-Stage Rotor B/Stator B Configuration; Third Stage is Test Stage.

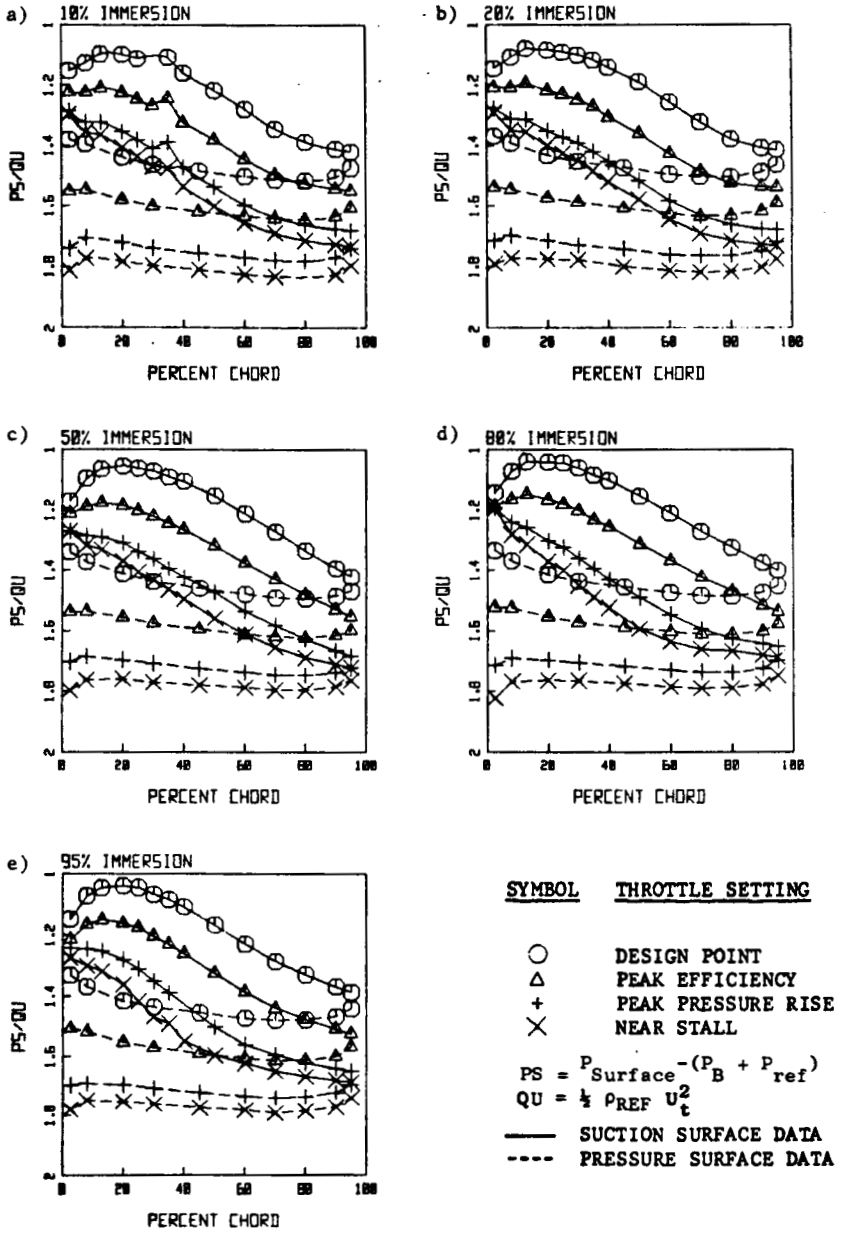

Figure 19. Stator Vane Surface Static Pressure Measurements for the 4-Stage Rotor B/Stator B Configuration; Third Stage is Test Stage.

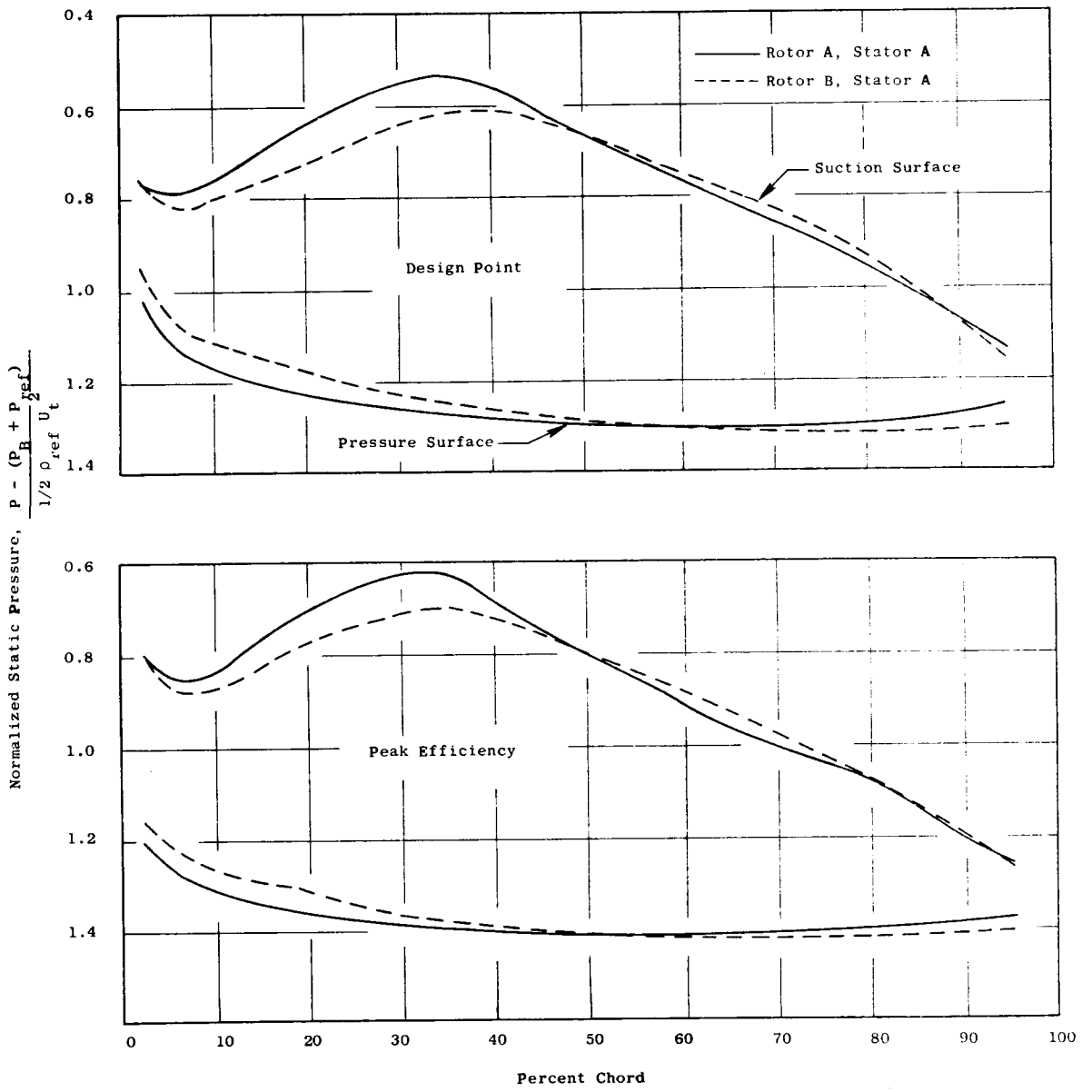

Figure 20. Comparison of Rotor Blade Surface Static Pressures at 5% Immersion.

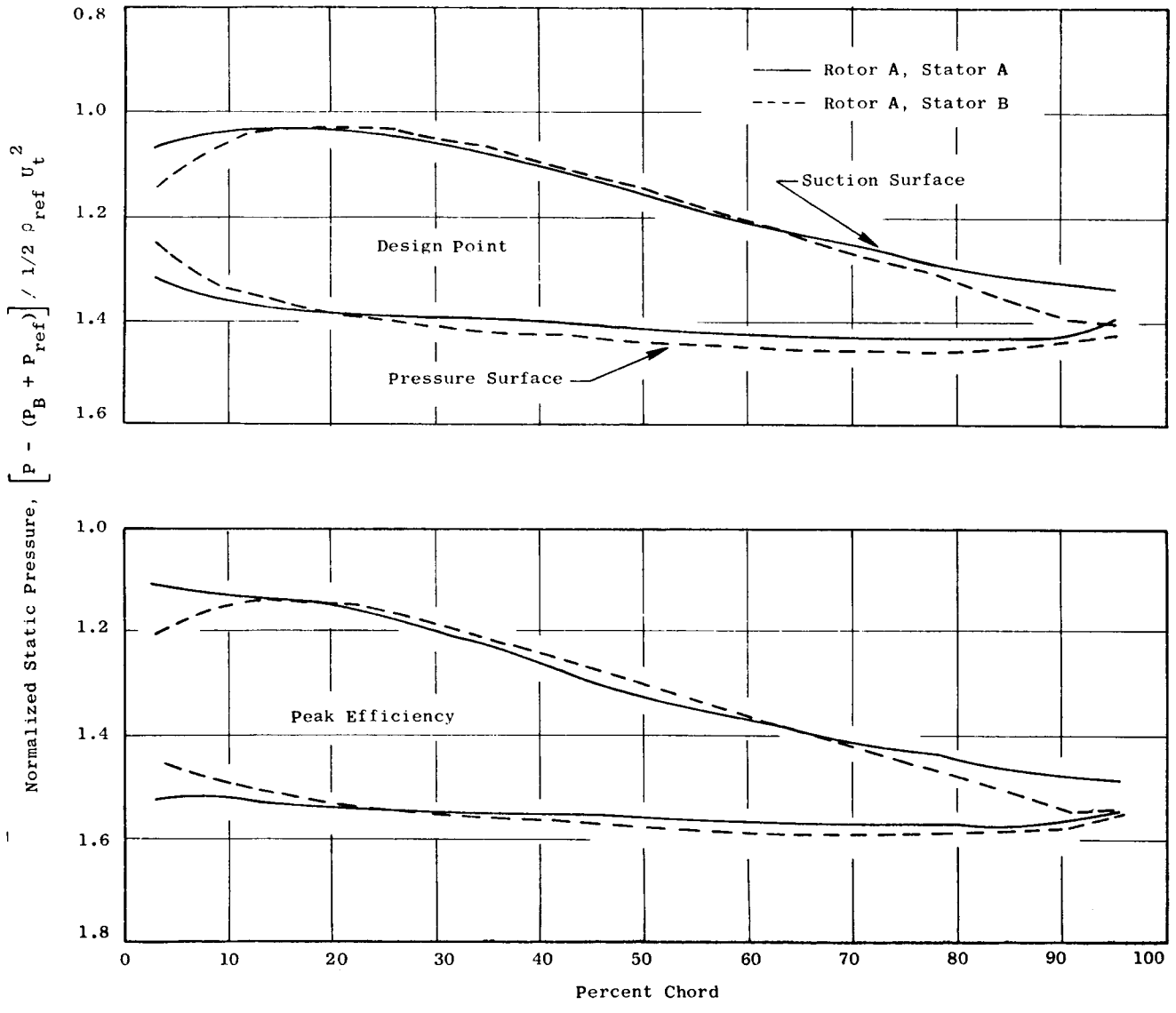

Figure 21. Comparison of Stator Surface Static Pressures at 95% Immersion.

4.3 COMPARISONS WITH POTENTIAL FLOW (CASC) SOLUTIONS

The velocity distributions along the suction and pressure surfaces of the blades and vanes were computed from the measured pressure distributions as discussed in Section 3.5. These velocity distributions were then compared with the potential flow CASC distributions. The results are presented in Figures 22 through 26. The spanwise locations of the CASC calculations did not always coincide with those of the static taps; the CASC immersions are indicated on the curves in these cases. All comparisons are made at the design point throttle setting.

Rotor A with Stators A, B, and C

Comparison of the experimentally determined surface velocities with the CASC velocities for Rotor A are shown in Figure 22. All of the test data for Rotor A running with Stators A, B, and C are presented in this Figure. In general, the test results are in qualitative agreement with CASC except at the tip section (Figure 22a). The pressure surface velocity distributions agree well with CASC at all immersions. Airfoil loadings near the leading edge, indicative of incidence angles, appear to be about as intended except near the hub where the leading edge loading is a little high (Figure 22d, e). The peak suction surface velocities occur at about the locations intended. There does appear to be slightly less suction surface velocity diffusion than intended on the aft portion of the blade from 80 percent immersion to the hub (Figure 22d and e).

The significant differences that are observed on the suction surface near the tip in Figure 22a are attributed to secondary flow/tip leakage effects (Reference 6). The suction surface velocity tends to be low from 5 percent to about 30 percent chord and high from 30 percent to 60 percent. These velocity perturbations are probably induced by the tip clearance vortex which moves away from the suction surface and away from the casing as percent chord increases.

Rotor B with Stators A and B

The comparisons of the experimentally determined surface velocities with the CASC velocities for Rotor B (shown in Figure 23) yield essentially the same results as for Rotor A except that leading edge loadings are lower. In fact, at 50 percent immersion (only), the 2.5 percent chord taps indicate a negative edge loading since the pressure velocity is higher than the suction velocity near the leading edge. Surface velocity distributions are in qualitative agreement with CASC except at the tip, and peak suction surface velocities occur about as intended. Suction surface velocity diffusion appears to be somewhat smaller than expected toward the trailing edge from 80 percent immersion to the hub (Figure 23d and e). Again, the effects of secondary flow and tip leakage are evident near the tip in Figure 23a.

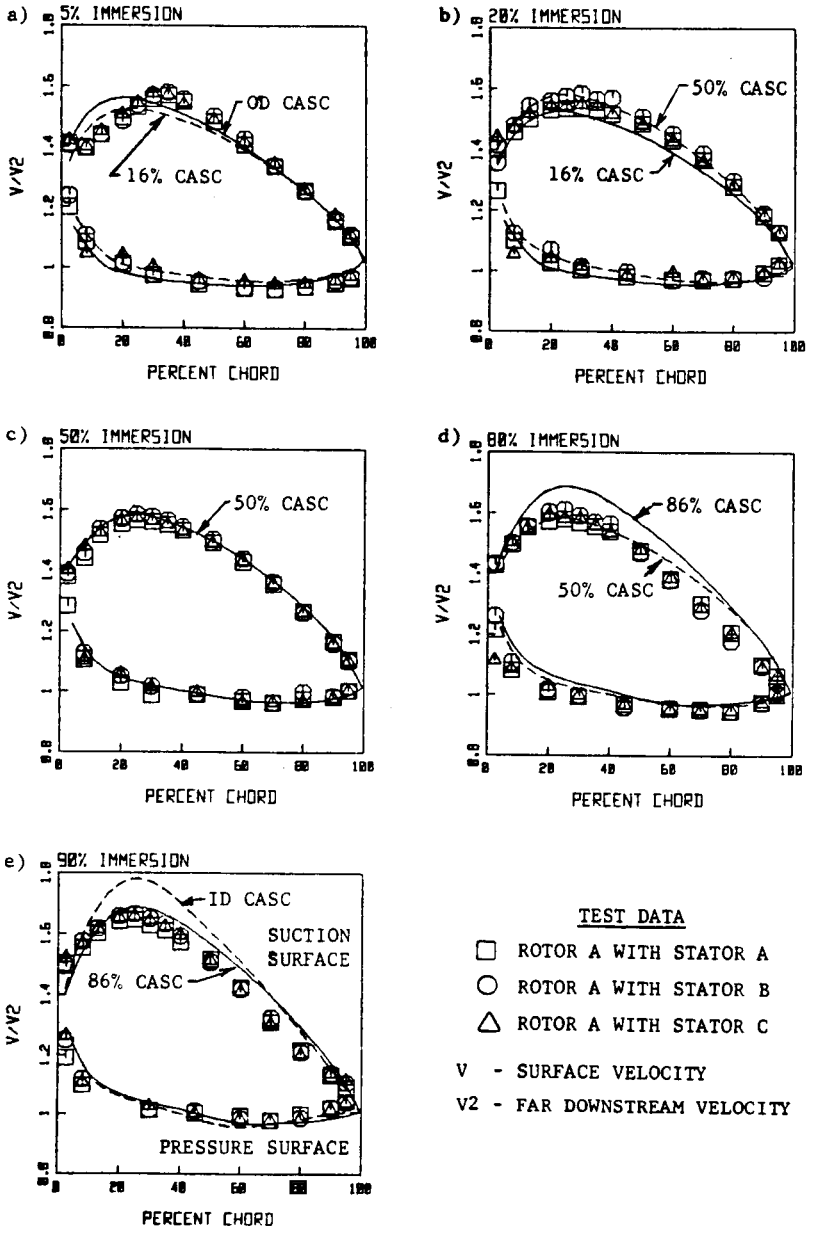

Figure 22. Rotor Blade Surface Velocity Distributions for Rotor A Operating Near the Design Point - Measurements Compared with Potential Flow CASC Solutions.

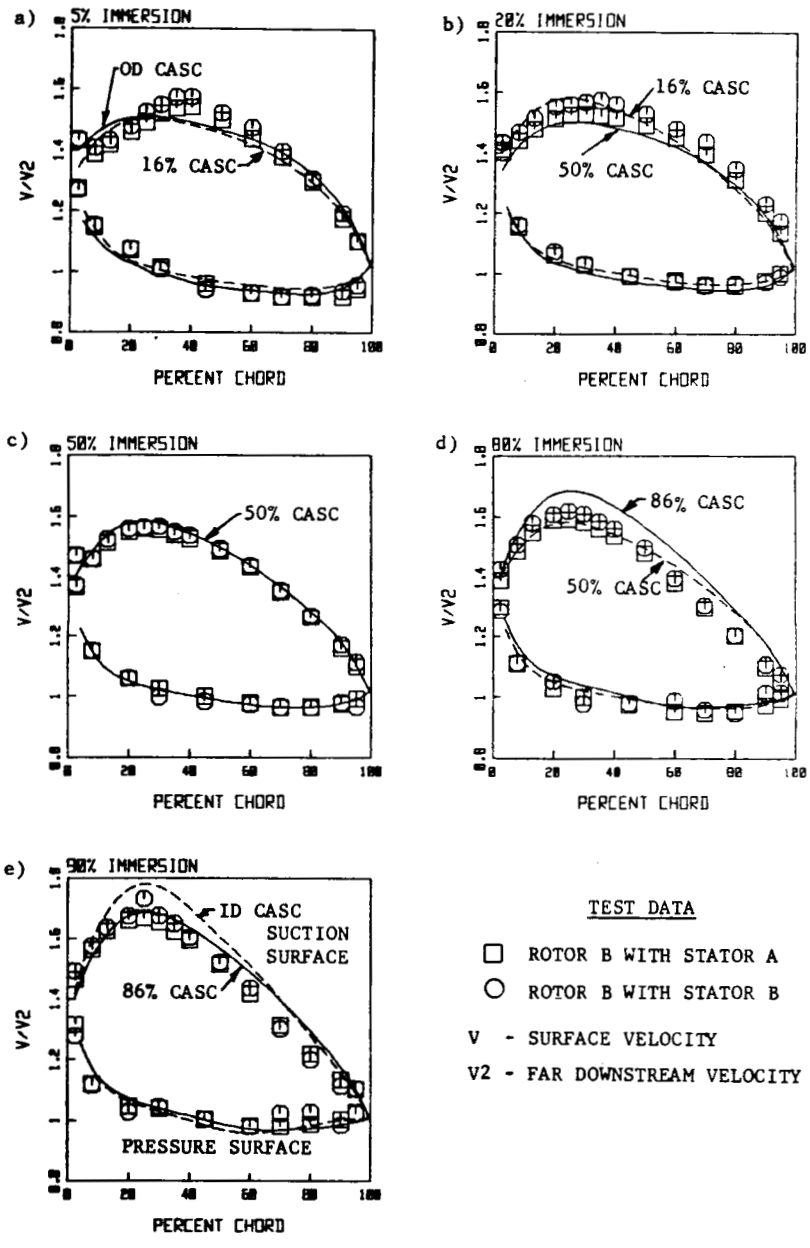

Figure 23. Rotor Blade Surface Velocity Distributions for Rotor B Operating Near the Design Point - Measurements Compared with Potential Flow CASC Solutions.

Stator A with Rotors A and B

Comparisons of the experimentally determined surface velocities with the CASC velocities for Stator A are shown in Figure 24. Airfoil loading near the leading edge is larger than predicted especially near the end walls and the velocity diffusion on the aft portion of the airfoil is less than predicted. Apparently the stator is operating at higher incidence angles (leading edge airfoil loadings) at the design point than expected. This would help to explain the large regions of separated flow found on the stator hub as the compressor is throttled toward stall.

Stator B with Rotors A and B

The comparisons of the experimentally determined surface velocities with the CASC velocities for Stator B are shown in Figure 25. The test results for the velocity distribution on the pressure surface are in qualitative agreement with CASC. The leading edge loadings for Stator B are lower than those for Stator A, especially near the hub, although they are still somewhat larger than intended. This could explain the improvement in the pressure-flow characteristic near stall obtained with Stator B (Figures 9 and 11). Airfoil loading is again less than predicted on the aft portion of the vane.

Stator C with Rotor A

Stator C data are shown in Figure 26. As before, pressure surface velocity distributions are in qualitative agreement with predictions. Airfoil leading edge loading is slightly larger than predicted near the endwalls. Except for the results at 50 percent immersion (Figure 26c), airfoil loading on the aft portion of the vane is less than predicted. The intended unloading of the aft portion of the vane near the endwalls is evident in Figures 26a and 26e. The high suction surface diffusion ratio (V_{max}/V_2) near the hub is probably responsible for the poorer peak efficiency observed with Stator C (see Figure 10).

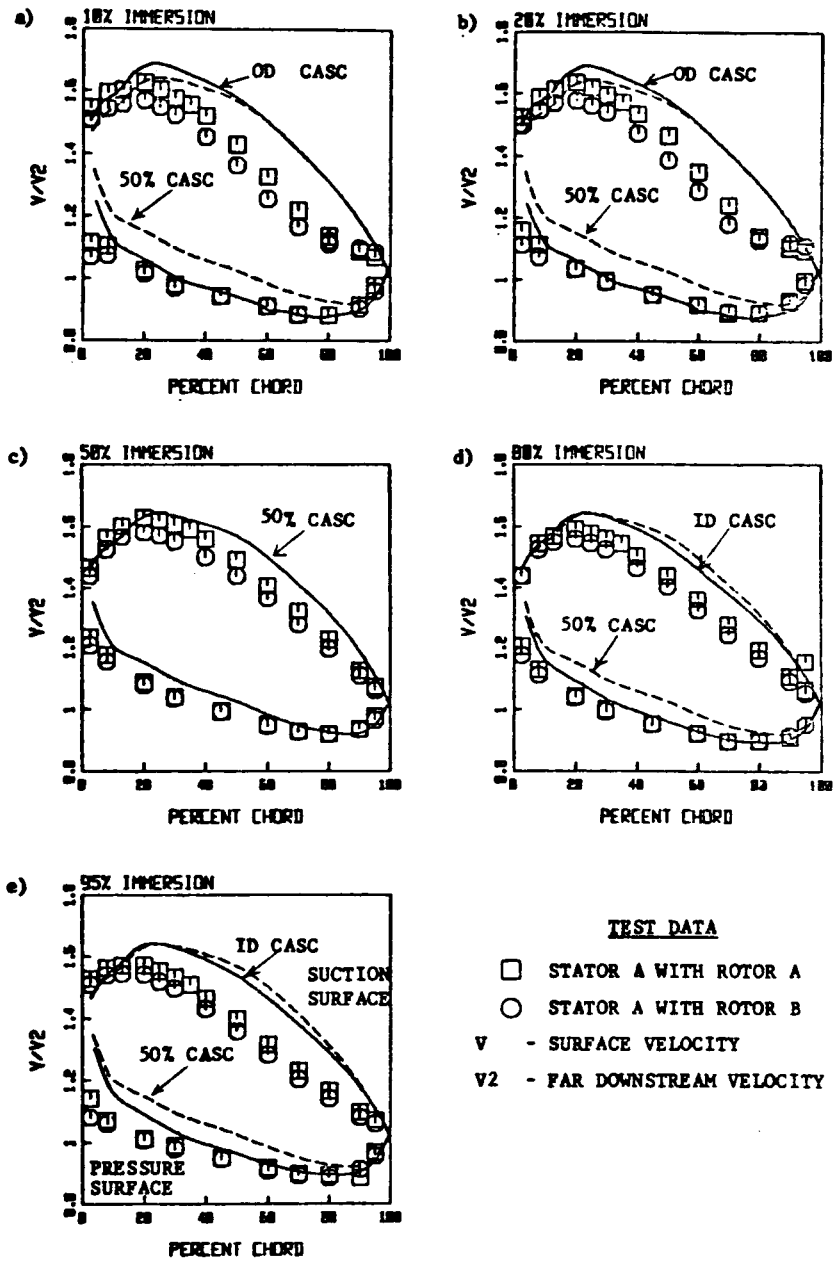

Figure 24. Stator Vane Surface Velocity Distributions for Stator A Operating Near the Design Point - Measurements Compared with Potential Flow CASC Solutions.

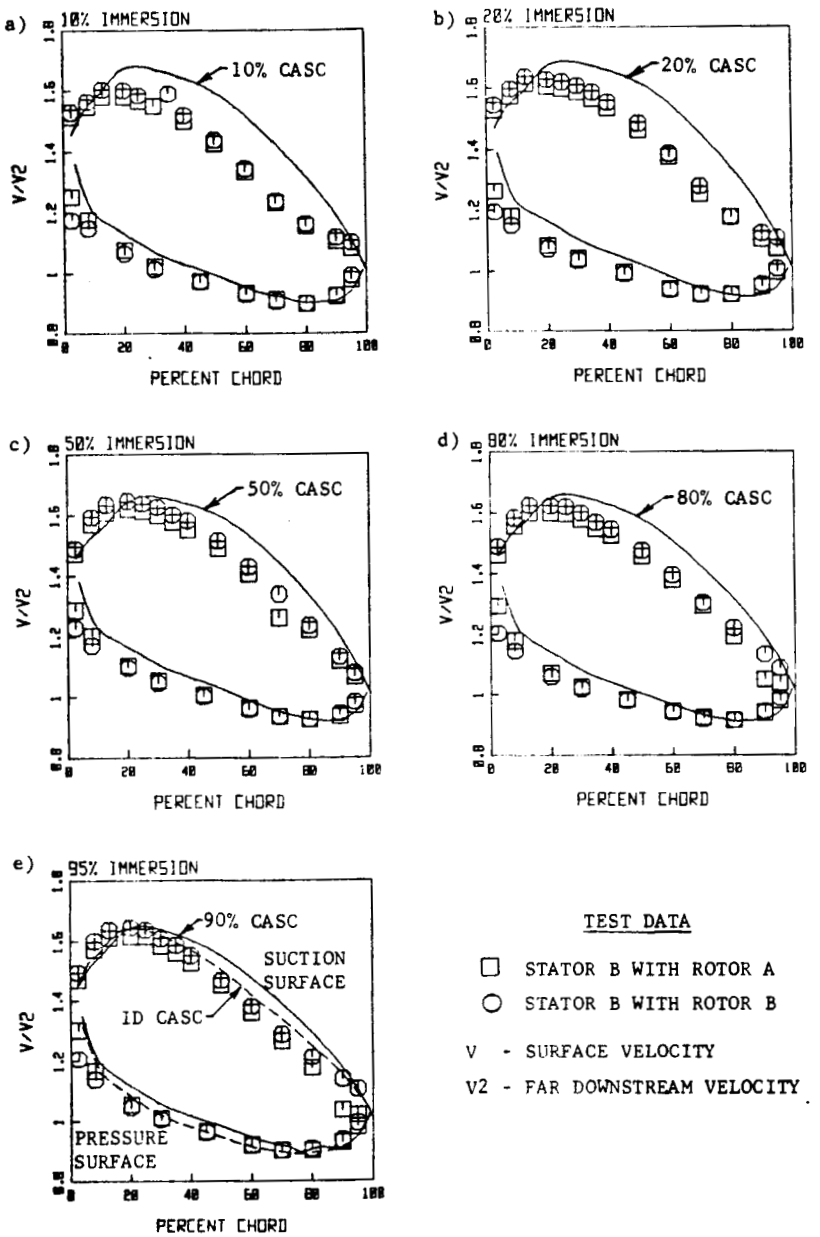

Figure 25. Stator Vane Surface Velocity Distributions for Stator B Operating Near the Design Point - Measurements Compared with Potential Flow CASC Solutions.

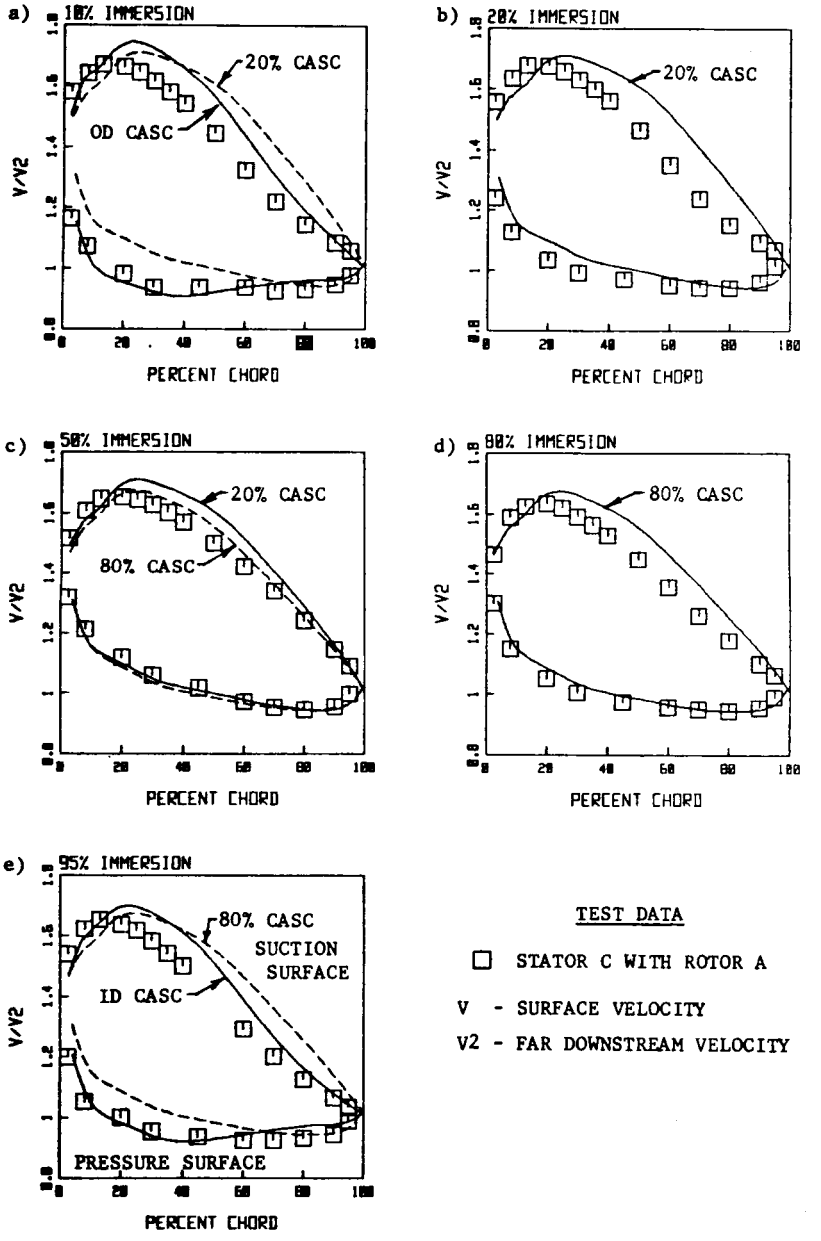

Figure 26. Stator Vane Surface Velocity Distributions for Stator C Operating Near the Design Point - Measurements Compared with Potential Flow CASC Solutions.

5.0 CONCLUSIONS

A series of short screening tests was conducted to determine the best rotor design and the best stator design of the several alternate designs which had the potential of reducing endwall losses relative to the Rotor A/ Stator A baseline design. The following test results were obtained:

- Rotor B tested with Stator A showed a 0.3 point improvement in efficiency at the design point relative to the baseline.

- Stator B tested with Rotor A showed a 0.4 to 0.5 point improvement in efficiency at the design point and a significant improvement in the pressure-flow characteristic near stall relative to the baseline. A 3.2 percent increase in peak pressure coefficient and 5.4 percent increase in flow range from the design point to the peak pressure rise point was obtained.

- Stator C tested with Rotor A showed a slight loss in efficiency at the design point relative to the baseline.

- Rotor B tested with Stator B showed a 0.3 to 0.4 point improvement in efficiency at the design point and a significant improvement in the pressure-flow characteristic near stall relative to the baseline. A 2.8 percent increase in peak pressure coefficient and a 5.4 percent increase in flow range from the design point to the peak pressure rise point was obtained.

- Even though the Rotor A/Stator B configuration showed very slightly better performance than the Rotor B/Stator B configuration, the Rotor B/Stator B configuration was selected as the "Best Stage", because of the possible beneficial effect of the Rotor B tip section at higher Mach numbers. This selection will allow both Rotor B and Stator B to undergo detailed testing.

6.0 LIST OF SYMBOLS AND ACRONYMS

Symbol	Definition
c	Stator shroud seal clearance
F_c	Compressibility correction factor
h	Annulus height
ID	Inside diameter
IGV	Inlet guide vane
OD	Outside diameter
P	Pressure
PS	Airfoil surface static pressure $\equiv P_{surface}-(P_B+P_{ref})$
QU	Normalizing quantity = $1/2\ P_{ref}U_t^2$
R	Radius
Re	Reynolds number
U_t	Wheel speed at tip
V	Air velocity
ϵ	Rotor tip clearance
η	Torque efficiency
ρ	Density
ϕ	Flow coefficient
ψ	Work coefficient ($\psi/4$ is four-stage average)
ψ'	Pressure coefficient ($\psi'/4$ is four-stage average)

Subscript

B	Barometer
C	Casing
H	Hub
ref	Reference
S	Static properties
T	Total properties
1	Upstream conditions
2	Downstream conditions

REFERENCES

1. Wisler, D.C., "Core Compressor Exit Stage Study, Volume I - Blading Design," NASA CR-135391, December 1977.

2. Wisler, D.C., "Core Compressor Exit Stage Study Volume II - Data and Performance Report for Rotor A/Stator A baseline Configurations," NASA CR-

3. Wisler, D.C., Koch, C.C., Smith, L.H., Jr., "Preliminary Design Study of Advanced Multistage Axial Flow Core Compressors," NASA CR-135133, February 1977.

4. Koch, C.C., and Smith, L.H., Jr., "Loss Sources and Magnitudes in Axial-Flow Compressors," Transitions of ASME, Journal of Engineering for Power, Vol. 98, Series A, No. 3, July 1976, page 411.

5. Brent, J.A., and Clemons, D.R., "Single-Stage Experimental Evaluation of Tandem-Airfoil Rotor and Stator Blading for Compressors," Final Report NASA CR-134713, November 1974.

6. Lakshminarayana, B., and Horlock, J.H., "Leakage and Secondary Flows in Compressor Cascades," R&M No. 3483, Dept. of Mechanical Engineering, University of Liverpool, London, England, March 1965.